Lipid transfer proteins initiate nuclear phosphoinositide signaling

Noah D. Carrillo[1,2,3], Mo Chen[1,3], Vincent L. Cryns[1,2,4,*] and Richard A. Anderson[1,4,*]

[1]University of Wisconsin Carbone Cancer Center, University of Wisconsin-Madison, School of Medicine and Public Health; 1111 Highland Avenue, Madison, WI 53705, USA
[2]Department of Medicine, University of Wisconsin-Madison, School of Medicine and Public Health; 1111 Highland Avenue, Madison, WI 53705, USA
[3]Co-first authors
[4]These authors contributed equally to this work
[*]Correspondence: vlcryns@medicine.wisc.edu; raanders@wisc.edu

Summary

The membrane-localized phosphatidylinositol (PI) 3-kinase (PI3K)/Akt pathway regulates cell growth and is aberrantly activated in cancer. Recent studies reveal a distinct nuclear PI3K/Akt pathway involving PI phosphate (PIP) kinases that bind the tumor suppressor protein p53 (wild-type and mutant) to generate nuclear p53-polyphosphoinositide (PIP_n) complexes that activate Akt. In the membrane pathway, PI transfer proteins (PITPs) transport PI, the precursor of PIP_ns, to endomembranes to enable PIP_n synthesis. In contrast, nuclear PIP_n signaling relies on poorly characterized non-membranous PIP_n pools. Here we show that PITPs accumulate in the non-membranous nucleoplasm in response to stress and are necessary to generate nuclear PIP_n pools. Class I PITPα/β bind p53 to form p53-PIP_n complexes that activate nuclear Akt in response to stress, which inhibits apoptosis. These findings demonstrate an unexpected function for PITPα/β in nuclear PIP_n signaling by generating membrane-free, protein-linked PIP_n pools that are modified by PIP kinases/phosphatases to regulate protein function.

Key words

Phosphoinositide; phosphatidylinositol transfer protein; PIP-linked protein, p53; $PI4,5P_2$; $PI3,4,5P_3$; nucleus

In brief

Phosphatidylinositol transfer proteins initiate the nuclear protein-associated PIP_n network in membrane-free regions.

Main text

Phosphoinositide lipids are synthesized from phosphatidylinositol (PI) in membranes by PI phosphate (PIP) kinases to produce a second messenger network comprised of seven distinct polyphosphoinositide (PIP_n) isomers. Class I PI 3-kinases (PI3K) catalyze the synthesis of $PI3,4,5P_3$, which leads to the recruitment and activation of the serine kinase Akt in membranes[1-7]. Akt in turn phosphorylates many substrates such as the FOXOs, TSC2, and BAD to promote cell growth and inhibit apoptosis[3]. This membrane-localized PI 3-kinase (PI3K)/Akt pathway is often hyperactivated in cancer and class I PI3K inhibitors are currently in the clinic[8, 9].

Akt is also activated in the nucleus[10-14]. Recent studies have identified a nuclear PI3K/Akt pathway distinct from the membrane-localized pathway that is dependent on p53[15, 16], a tumor suppressor protein that is frequently mutated in cancer[17, 18]. In this nuclear pathway, wild-type and mutant p53 are sequentially modified by PIP_ns and their associated PIP kinases (p53-PIP_n signalosome) in response to stress to synthesize p53-$PI3,4,5P_3$ complexes, which recruit and activate Akt in non-membranous nuclear structures[15, 16]. This nuclear Akt pathway is insensitive to PI3K inhibitors currently in the clinic[15], highlighting its therapeutic importance.

Although multiple PIP_ns and PIP kinases/phosphatases are present in the non-membranous nucleus[19-22], the mechanism by which the pool of nuclear PIP_ns is established is unknown. Unlike the most abundant nuclear phospholipid, phosphatidylcholine (PC), which is synthesized *in situ* in the nucleus[23-25], PI represents a minor fraction of nuclear phospholipids and is synthesized in the endoplasmic reticulum

(ER)[26] and connected nuclear envelope[27], suggesting that it is transported into the nucleoplasm. In the cytosol, PI is transported from the ER to membranes and between membranes by a family of lipid transfer proteins, the phosphatidylinositol transfer proteins (PITPs). The PITPs have not been implicated in nuclear transport or any functions in the nucleus. Intriguingly, PITPβ was reported to interact with p53 in a proteomics screen[28], prompting us to examine the potential functional role of PITPs in nuclear PIP_n signaling. Here we demonstrate that a subset of the PITP family are specifically required to generate the non-membranous nuclear PIP_n pools that is coupled to proteins by transporting PI into the nucleus. Significantly, within this PIP_n pool, PITPs bind p53 and initiate nuclear p53-PIP_n signaling, culminating in nuclear Akt activation and stress-resistance.

The nuclear localization of PITPs is regulated by cellular stress

The PITP family contains five members that are subdivided into two classes that exchange PI for PC (Class I, the single domain PITPα and PITPβ isoforms) or PI for PA (Class II, the multi-domain PITPNC1, PITPNM1, and PITPNM2 isoforms with C-terminal extensions)[29] (Fig. 1a). The most homologous members within the PITP family, PITPα/β/NC1, were expressed in the nucleus under basal conditions, and the nuclear levels of each isoform were increased by cisplatin coinciding with cisplatin-induced nuclear $PI4,5P_2$ increases as determined by immunofluorescence (IF) (Fig.1b,c and Extended Data Fig.1a). Confocal 3D sectioning (Extended Data Fig.1b-e) confirmed the enhanced nuclear levels of PITPα/β in response to genotoxic stress, which were observed in all cell lines tested regardless of tissue of origin or p53 mutational status (Fig. 1d and Extended Data Fig. 2a). Multiple cellular stressors (genotoxic, oxidative and

ferroptotic) increased the nuclear levels of PITPα/β, indicating a fundamental nuclear role for the PITPs in the cellular stress-response (Fig. 1e-f and Extended Data Fig. 2b). Moreover, stress induced the targeting of PITPs to the non-membranous nucleoplasm in all cell lines examined (Fig. 1g and Extended Data Fig. 2c and 3a-d).

PITPs regulate the nuclear PIP_n pool

All PIP_n isomers except $PI3,5P_2$ have been detected in the nucleus by multiple methods[15, 16, 19-21, 25, 30]. Among these, $PI4,5P_2$ forms distinctive nuclear foci that colocalize with nuclear speckle markers in regions devoid of membranes[15, 16, 20, 21, 31]. PI is the precursor of all PIP_ns[32] and together with our observation that cellular stress induces the nuclear localization of PITPs, we investigated the role of PITPs in regulating the nuclear PIP_n pool. Silencing PITPα or PITPβ reduced basal and stress-induced nuclear $PI4,5P_2$ levels, while combined knockdown (KD) of both PITPα and PITPβ further decreased nuclear $PI4,5P_2$ levels compared to the individual KD (Fig. 2a,b). PITPNC1 KD resulted in a modest reduction of basal and stress-induced nuclear $PI4,5P_2$ levels (Fig. 2a,b). Combined KD of PITPα and PITPβ robustly suppressed stress-induced nuclear levels of PI4P and $PI3,4,5P_3$ (Fig. 2c,d). Moreover, combined KD of PITPα and PITPβ inhibited stress-induced nuclear $PI4,5P_2$ generation in transformed and untransformed cells independent of p53 mutational status (Fig. 2e-g and Extended Data Fig. 3e). These results demonstrate that PITPs are necessary to generate the nuclear PIP_n pools (Fig. 2h).

PITPα/β bind p53 and their interaction is regulated by cellular stress

Together with the reported interaction of PITPβ and p53[28], the role of PITPs in regulating nuclear PIP_n levels suggested PITPs might play a functional role in generating nuclear p53-PIP_n complexes. To explore this, we investigated the interaction of p53 with all five PITPs using multiple approaches. Proximity ligation assay (PLA)[30] demonstrated class I, but not class II PITPs, associated with mutant p53 ($p53^{mt}$) and wild-type p53 ($p53^{wt}$) in the nucleus, and that their association was enhanced by cisplatin (Fig. 3a,b and Extended Data Fig. 4a-c). Notably, the association of PITPα/β with $p53^{wt}$ was minimal under basal conditions and dramatically increased by stress, while PITPα/β associated constitutively with $p53^{mt}$ with a modest increase in response to stress. Similar to the nuclear localization of PITPs (Fig. 1g and Extended Data Fig. 1a-e and 3a-d), the PITPα/β-p53 PLA complexes were present in the nucleoplasm in regions distinct from the nuclear envelope (Fig. 3c and Extended Data Fig. 4d-f).

The PITPα/β-p53 complex was next examined by immunoprecipitation (IP). Consistent with the PLA data, class I, but not class II PITPs, bound $p53^{wt}$ and $p53^{mt}$ and these interactions were increased by stress in all cells examined (Fig. 3d-f, h-i and Extended Data Fig. 5a-n). Although nuclear levels of PITPα/β and PITPNC1 increased in response to stress (Fig.1b-c and Extended Data Fig. 1a), the interaction with p53 was specific for the class I PITPs, indicating specificity within the family. Moreover, the small heat shock proteins (sHSPs) Hsp27 and αB-crystallin, which stabilize the p53-PIP_n complex[16], are also stress-regulated components of the PITPα/β-p53 complex (Fig. 3d,g,h,j,k). Additionally, *in vitro* binding studies with recombinant PITPα/β proteins pulled down by p53 demonstrated a high-affinity, saturable binding of class I PITPs to p53 (Fig. 3l-o).

Collectively, these data show that PITPα/β form a nuclear complex with p53 in response to stress (Fig. 3p).

PITPα/β regulate PIP_n binding to p53 and other protein targets

As PITPα/β regulate nuclear PIP_n levels and bind p53 in the nucleus, we examined the potential role of PITPα/β in regulating the PIP_n interactions with p53, which stabilize p53[16]. Single or combined KD of PITPα/β, but not PITPNC1, reduced or largely eliminated, respectively, $p53^{mt}$-$PI4,5P_2$ and $p53^{mt}$-$PI3,4,5P_3$ complexes detected by PLA; combined KD of PITPα/β disrupted p53mt-PIP_n complexes to a similar degree as p53 KD (Fig. 4a-c). Similar results were observed in $p53^{wt}$ cells: individual or combined PITPα/β KD inhibited $p53^{wt}$-$PI4,5P_2$ and $p53^{wt}$-$PI3,4,5P_3$ complexes (Fig. 4d-f). We next quantified the PIP_n isoforms linked to p53 by p53-IP followed by simultaneous Western blotting (WB) with antibodies (Abs) against specific PIP_n isoforms detected with fluorescently labeled secondary Abs (IP fluorescent-WB). KD of PITPα or PITPβ markedly reduced the PI4P, $PI4,5P_2$ and $PI3,4,5P_3$ that co-IPed with $p53^{mt}$ in response to genotoxic stress, while the combined KD largely eliminated all PIP_ns associated with $p53^{mt}$ (Fig. 4g-j). Single or combined PITPα/β KD also inhibited cisplatin-stimulated $p53^{wt}$-$PI4,5P_2$ complex formation (Fig. 4k,l). These findings indicate that PITPα/β play a key role in coupling PIP_ns to $p53^{wt}$ and $p53^{mt}$ proteins in response to stress.

Consistent with reported role of PIP_n binding to stabilize p53[16], KD of PITPα or PITPβ, but not PITPNC1, modestly reduced $p53^{mt}$ levels in cells under basal and stressed conditions, while the combined KD of PITPα and PITPβ robustly suppressed $p53^{mt}$ levels (Fig. 5a). The induction of $p53^{wt}$ by cisplatin was also markedly inhibited by individual PITPα/β KD

and completely abrogated by combined PITPα/β KD (Fig. 5b). Additionally, individual and combined KD of PITPα/β robustly reduced protein-bound PI4,5P_2 levels in the whole cell lysate and PI4,5P_2 bound to p53^{mt} in response to stress (Fig. 5c,d). Furthermore, KD of PITPα/β (individual or combined), but not PITPNC1, reduced levels of multiple protein-bound PIP$_n$s (PI4P, PI4,5P_2 and/or PI3,4,5P_3) in whole cell lysates (Fig. 5b-f). Intriguingly, WB of whole cell lysates with Abs specific for PI4P, PI4,5P_2 or PI3,4,5P_3 revealed many protein bands, including some that were enhanced by genotoxic stress (Fig. 5b,c,e). Single or combined KD of PITPα/β, but not PITPNC1, diminished the intensity of these other protein bands, indicating that these PITPs may regulate PIP$_n$ association with multiple cellular proteins. Taken together, these findings indicate that class I PITPs mediate the stress-responsive association of PIP$_n$s with p53 and other proteins (Fig. 5g), which constitute the membrane-free nuclear PIP$_n$ pools.

PITPα/β regulate p53-PIP$_n$ signalosome formation and nuclear Akt activation to inhibit stress-induced apoptosis

The p53-PIP$_n$ signalosome is regulated by cellular stress, leading to the formation of p53-PI3,4,5P_3 complexes that recruit and activate Akt in the nucleus and protect cells from stress-induced apoptosis[15]. The identification of class I PITPs as upstream regulators of p53-PIP$_n$ complex assembly implicates these lipid transfer proteins in nuclear Akt activation. Consistent with this concept, individual KD of PITPα or PITPβ, but not PITPNC1, suppressed stress-induced nuclear Akt activation quantified by nuclear pAkt^{S473} IF, and combined PITPα/β KD resulted in a more robust inhibition (Fig. 6a,b). Similar results were obtained with multiple human cancer cell lines expressing p53^{mt} (Fig.

6c-e and Fig. 2e). KD of $p53^{mt}$, PITPα or PITPβ, but not PITPNC1, moderately reduced cell viability under basal conditions and sensitized cells to cisplatin treatment, while combined PITPα/β KD further decreased cell viability (Fig. 6f,g and Extended Data Fig. 6a-g). The cytotoxicity of $p53^{mt}$ and PITPα/β KD was associated with a corresponding increase in caspase 3 activity (Fig. 6h and Extended Data Fig. 6e-j), indicating that the loss of PITPα/β triggers apoptosis and sensitizes cells to genotoxic stress. These findings underscore the regulation of nuclear Akt activation by PITPα/β which confers resistance to genotoxic stress-induced apoptosis.

As PITPα/β exchange PI for PC, we next investigated whether their PI transfer activity was required to regulate nuclear PIP_n pools and nuclear Akt activation. To this end, we utilized the PITPα/β T59D mutant that specifically disrupts PI binding[33-35]. Ectopically expressed $PITPα/β^{wt}$ interacted with $p53^{wt}$ and mutant $p53^{R175H}$, while the corresponding PITPα/β T59D mutants exhibited severely impaired binding to p53 (Fig. 7a and Extended Data Fig. 7a-c). Moreover, the reduction in the stress-induced nuclear $PI4,5P_2$ pool and nuclear $pAkt^{S473}$ levels by combined PITPα and PITPβ KD using pooled siRNAs targeting their 3'-UTR was rescued by expression of $PITPα^{wt}$, but not mutant T59D PITPα (Fig. 7b-e). Notably, the nuclear $PI4,5P_2$ and $pAkt^{S473}$ levels correlated with the re-expressed levels of $PITPα^{wt}$, but not mutant T59D PITPα (Fig. 7f-i), indicating that these phenotypes are dose-dependent. The cytotoxicity and sensitization to cisplatin-induced apoptosis by combined PITPα/β KD using the 3'-UTR targeting siRNAs were partly rescued by re-expressing $PITPα^{wt}$ but not the T59D mutant (Fig. 7j,k and Extended Data Fig. 7d). Combined PITPα/β KD also inhibited EGF-stimulated cell invasion and these effects were partly restored by re-expressing $PITPα^{wt}$ but not the T59D mutant (Fig. 7l,m). These

results demonstrate that the PI transfer activity of class I PITPs regulates their interaction with p53 and related nuclear Akt activation. The data also suggests a broader role for PITPα/β in functional protein interactions beyond p53 that contribute to cell growth, invasion and protection against genotoxic stress (Fig. 7n).

Discussion

Here we reveal an unexpected role for class I PITPα/β in generating the nuclear PIP_n pools that initiate nuclear PIP_n signaling. Although the existence of nuclear PIP_ns and their role in the cell cycle[36], oxidative stress[21, 37-42] and the DNA damage response[15, 43-45] is supported by emerging evidence[21], the molecular origin and regulation of nuclear PIP_ns in regions devoid of membranes have been enigmatic[46]. PITPs have a well-established role in transporting PI from the endoplasmic reticulum to membranes to enable membrane-localized PIP_n signaling via PIP kinases, phosphatases and phospholipase-C[23-26, 29, 47]. The findings presented here demonstrate that multiple PITPs accumulate in the non-membranous nucleoplasm in response to diverse cellular stressors to regulate the membrane-free nuclear PIP_n pools. As such, these data greatly expand the known lipid transport activities of these proteins that were thought to act largely in the cytosol and establish the mechanistic basis for nuclear PIP_n pools.

In addition to generating a nuclear pool of PIP_ns available for signaling, PITPα/β, but not other PITP family members, bind directly to $p53^{wt}$ and $p53^{mt}$ in response to stress. This complex also includes the small heat shock proteins (Hsp27 and αB-crystallin), which stabilize p53[16]. PITPα/β binding to p53 controls the interaction of PIP_ns with p53 (p53-PIP_n signalosome), which is catalyzed by multiple PIP kinases and phosphatases,

culminating in the formation of p53-PI3,4,5P_3 complexes. p53-PI3,4,5P_3, in turn, recruits and activates Akt in the nucleus, conferring resistance to stress-induced apoptosis. Notably, these activities of PITPα/β require PI binding, underscoring the critical functional role of lipid transport in nuclear PIP_n signaling. Indeed, the ability of WT PITPα, but not a PI binding-defective mutant, to rescue the phenotype of combined PITPα/β KD suggests a functional redundancy in the respective contributions of PITPα and PITPβ to nuclear phosphoinositide signaling. This is consistent with previous reports that either PITPα or PITPβ is sufficient to rescue the phenotype of double PITPα/β knockout in a PI-binding dependent manner[33, 48]. Overall, these data point to an unequivocal function for PITPα/β in nuclear phosphoinositide signaling by directly transferring PI to p53 to initiate p53-PIP_n signaling.

Remarkably, PITPα/β also regulate the coupling of PIP_ns to a suite of cellular proteins beyond p53 detected by WB with antibodies specific for individual PIP_n isomers. These findings suggest a “third messenger” pathway with p53 as the founding member whereby PIP_n second messengers are linked to cellular proteins in membrane-free regions and modified by PIP kinases/phosphatases to regulate their function (Fig. 7n). Indeed, the assembly of distinct PIP_n isomer-protein complexes with unique binding partners has the potential to enable exquisite spatial and temporal regulation of signaling cascades anchored on cellular proteins instead of membranes. Given the critical role of class I PITPs in initiating nuclear phosphoinositide signaling, which attenuates cellular stress and apoptosis, these findings also point to these PITPs as potential therapeutic targets in a variety of diseases including cancer.

ACKNOWLEDGMENTS

We thank Dr. Adrea Galmozzi for discussions and comments, and Lance Rodenkirch for technical support. N.D.C. is supported by a National Institutes of Health T32 Training Grant 5T32ES007015-43 to the Molecular and Environmental Toxicology graduate training program at UW-Madison. This work was supported in part by a National Institutes of Health grant R35GM134955 (R.A.A.), Department of Defense Breast Cancer Research Program grants W81XWH-17-1-0258 (R.A.A.), W81XWH-17-1-0259 (V.L.C.) and W81XWH-21-1-0129 (V.L.C.), and a grant from the Breast Cancer Research Foundation (V.L.C.).

AUTHOR CONTRIBUTIONS

M.C., N.D.C, V.L.C., and R.A.A. designed the experiments. N.D.C. and M.C. performed the experiments. N.D.C., M.C., V.L.C., and R.A.A. wrote the manuscript.

DECLARATION OF INTERESTS

Authors declare that they have no competing interests.

METHODS

Cell culture and constructs

A549, BT-549, Cal33, HCT116, HS578T, MDA-MB-231, SUM159, SUM1315, HEK293FT, and MCF-10A cells were purchased from ATCC. MCF10A cells were cultured in DMEM/F12 (#11330-032, Invitrogen) supplemented with 10% fetal bovine serum

(#SH30910.03, Hyclone), 1% penicillin/streptomycin (#15140-122, Gibco), 20 ng/mL EGF (#CC-4107, Lonza), 0.5 mg/mL Hydrocortisone (#H4001, Sigma), 100 ng/mL Cholera toxin (#C-8052, Sigma), and 10 µg/mL Insulin (#I-1882, Sigma). The other cells were maintained in DMEM (#10-013-CV, Corning) supplemented with 10% fetal bovine serum (#SH30910.03, Hyclone) and 1% penicillin/streptomycin (#15140-122, Gibco). The cell lines used in this study were routinely tested for mycoplasma contamination using MycoAlert Mycoplasma Detection Kit (#LT07-318, Lonza), and mycoplasma-negative cells were used. None of the cell lines used in this study are listed in the database of commonly misidentified cell lines maintained by ICLAC. The p53 Flag-tagged wild-type and R175H mutant constructs used for this work were described previously[16]. The HA-tagged wild-type PITPα/β constructs and PI-binding deficient mutants T59D[33] were purchased from Genscript. Constructs were transfected in mammalian cells by the lipid-based delivery system from Invitrogen (Lipofectamine™3000, #L3000015, Thermo Fisher Scientific) according to the manufacturer's instructions. Typically, 2-5 µg of DNA and 6-10 µl of lipid were used for transfecting cells in 6-well plates. Cells with at least 80% transfection efficiency were used for further analysis.

Antibodies and reagents

Monoclonal antibodies against p53 (clone DO-1, #SC-126, Santa Cruz Biotechnology), p53 (clone 7F5, #2527, Cell Signaling), pAkt^{S473} (clone 193H12, #4058, Cell Signaling), HA-tag (clone C29F4, #3724, Cell Signaling), Flag-tag (clone D6W5B, #14793, Cell Signaling), GAPDH (clone 0411, #sc-47724, Santa Cruz Biotechnology), Lamin B2 (clone D8P3U, #12255, Cell Signaling), EGFR (clone D6B6, #2085, Cell Signaling), HSP27

(clone D6W5V, #95357, Cell Signaling), and polyclonal antibodies against PITPα (#16613-1-AP, ThermoFisher), PITPβ (#ab127563, abcam), PITPNC1 (IF, #ab222078, abcam), PITPNC1 (WB, #NBP2-19842, Novus), PITPNM1 (#26983-1-AP, Proteintech), PITPNM2 (#PA5-48616, Invitrogen), and αB-Crystallin (#ADI-SPA-223-F, Enzo) were used in this study. For conventional immunostaining and PLA analysis of phosphoinositides, anti-PI4P (#Z-P004), PI4,5P_2 (#Z-P045) and PI3,4,5P_3 (#Z-P345) antibodies were purchased from Echelon Biosciences. For immunoblotting analyses, antibodies were diluted at a 1:1000 ratio except for p53 (clone DO-1, 1:5000) and GAPDH (clone 0411, 1:5000). For immunoprecipitation, antibody-conjugated agarose was purchased from Santa Cruz Biotechnology, including agarose-conjugated antibodies against p53 (#sc-126AC), PITPα/β (#sc-398050AC), HA-tag (#sc-7392AC), and Flag-tag (#sc-166355AC). For immunostaining analyses and proximity ligation assay (PLA), antibodies were diluted at a 1:100 ratio. Nuclear envelope marker (Alexa Fluor®488 Lamin A/C, clone 4C11, #8617, Cell Signaling, 1:200) was used to examine subnuclear regions. For the knockdown (KD) experiments, the ON-TARGETplus siRNA SMARTpool with 4 siRNAs in combination against human p53 (#L-003329-00), PITPα (#L-018010-00), PITPβ (#L-006459-01), and PITPNC1 (#L-012476-02) were purchased from Dharmacon. Non-targeting siRNA (Dharmacon) was used as a control. For the KD and rescue experiments, pooled-siRNAs targeting the 3'UTR of PITPα (sense 5'-AGGCAACUUUCGAUUCCUUACUGUA-3' and antisense 5'-UACAGUAAGGAAUCGAAAGUUGCCU-3'; sense 5'-CCGUCUCUCUCCAUUGUGUUCCGAU-3' and antisense 5'-AUCGGAACACAAUGGAGAGAGACGG-3') and pooled-siRNAs targeting the 3'UTR of

PITPβ (sense 5'- GAGUGAACAACAAUCUGACCAGUAU-3' and antisense 5'-AUACUGGUCAGAUUGUUGUUCACUC-3'; sense 5'- CUACAAAGCUGAUGAAGAC-3' and antisense 5'-GUCUUCAUCAGCUUUGUAG-3') were purchased from Thermo Fisher Scientific. The siRNAs were delivered to cells by RNAiMAX reagent (#13778150, Thermo Fisher Scientific), and KD efficiency was determined by immunoblotting. KD efficiency greater than 80% was required to observe phenotypic changes in the study. Cisplatin, (#NC1706394, Fisher Scientific), etoposide (#S1225, Sellekchem), Erastin (#S7242, Selleckchem), tert-Butylhydroquinone (tBHQ, #SPCM-T1540-06, Spectrum), and hydroxyurea (HU, #1332000, Millipore Sigma) were used as cellular stressors.

Immunoprecipitation and immunoblotting

Cells were removed from the medium after the indicated treatment, washed three times with ice-cold PBS, and lysed in an ice-cold RIPA lysis buffer system (#sc-24948, Santa Cruz Biotechnology) with 1 mM Na_3VO_4, 5 mM NaF, and 1x protease inhibitor cocktail (#11836153001, Roche). The cell lysates were then sonicated at 15% amplitude for 15 s. After sonication, the cell lysates were incubated at 4°C with continuous rotation for 1 h and subsequently centrifuged at maximum speed for 10 min to collect the supernatant. The protein concentration in the supernatant was measured by the Bradford protein assay (#5000201, BIO-RAD) according to the manufacturer's instructions. Equal amounts of protein were used for further analysis. All antibodies were diluted at a 1:1000 ratio for immunoblotting unless otherwise indicated. For immunoprecipitation, 0.5-1 mg of protein was incubated with 20 µl of antibody-conjugated agarose (Santa Cruz Biotechnology) at 4°C for 24 h. After washing five times with lysis buffer, the protein complex was eluted

with SDS sample buffer. For immunoblotting, 5-20 µg of protein were loaded. For immunoblotting of immunoprecipitated complexes, horseradish peroxidase (HRP)-conjugated antibodies were used to avoid non-specific detection of immunoglobulin in the immunoprecipitated samples. HRP-conjugated p53 (#sc-126HRP), PITPα (#sc-13569HRP), PITPβ (#sc-390500HRP) antibodies were purchased from Santa Cruz Biotechnology. Immunoblots were developed by Odyssey Imaging System (LI-COR Biosciences) and the intensity of protein bands was quantified using ImageJ. The unsaturated exposure of immunoblot images was used for quantification with the appropriate loading controls as standards. Statistical data analysis was performed with Microsoft Excel, using data from at least three independent experiments.

Fluorescent IP-WB

Cells were lysed in a RIPA lysis buffer system after the indicated treatment and quantified for protein concentration as described above. For endogenous p53 or FLAG-tagged p53 immunoprecipitation, 0.5-1 mg of cell lysates were incubated with 20 µl anti-p53 (#sc-126 AC, Santa Cruz Biotechnology) or anti-FLAG (#sc-166355AC, Santa Cruz Biotechnology) mouse monoclonal IgG antibody-conjugated agarose at 4°C for 24 h. Normal immunoglobulin (IgG)-conjugated agarose was used as a negative control (#sc-2343, Santa Cruz Biotechnology). After washing three times with PBST (PBS with 0.1% Tween 20), the protein complex was eluted with SDS sample buffer. The sample was then boiled at 95°C for 10 min. For immunoblotting, 5-20 µg of protein were loaded. The protein complexes associated with p53 were resolved by SDS-PAGE and transferred onto a PVDF membrane (#IPVH00010, MilliporeSigma). The membrane was blocked with 1%

BSA in TBS for 1 h at room temperature. For double fluorescent IP-WB detecting p53-PI4P/PI4,5P_2/PI3,4,5P_3 complexes, anti-p53 rabbit monoclonal IgG antibody (clone 7F5, #2527, Cell Signaling) at 1:2000 dilution and anti-PI4P mouse monoclonal IgM antibody (#Z-P004, Echelon Biosciences), PI4,5P_2 mouse monoclonal IgM antibody (#Z-P045, Echelon Biosciences), or PI3,4,5P_3 mouse monoclonal IgM antibody (#Z-P345, Echelon Biosciences) at 1:1000 dilution were mixed together in blocking buffer with 0.02 % Sodium Azide and incubated with the membrane at 4°C overnight. The next day, the membrane was washed three times with TBST for 10 min each time. For the secondary antibody incubation, goat anti-rabbit IgG antibody conjugated with IRDye 800CW fluorophore (#926-32211, LI-COR) detectable on the 800 nm wavelength channel of the Odyssey Fc Imaging System (LI-COR Biosciences) and goat anti-mouse IgM antibody conjugated with IRDye 680RD fluorophore (#926-68180, LI-COR) detectable on the 700 nm wavelength channel at 1:10000 dilution were mixed in blocking buffer with 0.01 % SDS and 0.1% Tween 20 and incubated with the membrane at room temperature for 2 h. The membrane was then washed three times with TBST for 10 min each time. The images were subsequently acquired simultaneously using the 700 and 800 nm wavelength channels on the Odyssey Fc Imaging System (LI-COR Biosciences). The p53-associated PI4P/PI4,5P_2/PI3,4,5P_3 complex was visualized by overlapping the 700 and 800 nm channels. Statistical data analysis was performed with Microsoft Excel, using data from at least three independent experiments.

***In vitro* binding assay**

The recombinant proteins p53 (#81091, Active Motif), PITPα (#ab101666, Abcam), PITPβ (#LS-C794864, LSBio) were used for *In Vitro* binding assays. The binding assay was performed in PBST by incubating a constant amount of p53 with an increasing amount of PITPα/β in the presence of 20 µl anti-p53 antibody-conjugated agarose (#sc-126AC, Santa Cruz). After incubating overnight at 4°C, unbound proteins were removed by washing three times with PBST, and the protein complex was analyzed by immunoblotting.

Immunofluorescence (IF) and Confocal Microscopy

For immunofluorescence studies, cells were grown on coverslips coated with 0.2 % gelatin (#G9391, MilliporeSigma). Cells were fixed with 4% paraformaldehyde (PFA) (#sc-281692, Santa Cruz Biotechnology) for 20 min at room temperature followed by washing three times with PBS. Next, the cells were permeabilized with 0.3% Triton-X100 for 30 min to thoroughly permeate the nuclear envelope and rewashed three times with PBS. The cells were then blocked with 1% BSA in PBS for one hour at room temperature. After blocking, cells were incubated with primary antibodies overnight at 4ºC. The cells were then washed three times with PBS and incubated with fluorescent-conjugated secondary antibodies (Molecular Probes) for 1 hour at room temperature. After secondary antibody incubation, the cells were washed three times. Then the coverslips were taken out from the dishes, air-dried for 10 min at room temperature and mounted in Prolong™ Glass Antifade Mountant with NucBlue™ Stain (#P36985, Thermo Fisher Scientific). The images were taken by Leica SP8 3xSTED Super-Resolution Microscope, which is both a point scanning confocal and 3xSTED super-resolution microscope. The Leica SP8 3xSTED microscope was controlled by LASX software (Leica Microsystems). All images

were acquired using the 100X objective lens (N.A. 1.4 oil). The z-stack images were taken with each frame over a 0.2 µm thickness. For quantification, the mean fluorescent intensity of channels in each cell was measured by LASX. GraphPad Prism Version 9.4.1 generated quantitative graphs. The images were processed using ImageJ. The correlation of double staining channels was quantified by GraphPad Prism using Pearson's correlation coefficient (Pearson's r), ranging between 1 and −1. A value of 1 represents perfect correlation, 0 means no correlation, and -1 means perfect negative correlation[49]. Pearson's r greater than 0.7 suggests a strong correlation[50].

Proximity Ligation Assay (PLA)

PLA was utilized to detect *in situ* protein-protein/PI interaction as previously described [15, 16, 30]. After fixation and permeabilization, cells were blocked before incubation with primary antibodies as in routine IF staining. The cells were then processed for PLA (#DUO92101, MilliporeSigma) according to the manufacturer's instruction and previous publications [15, 16, 30]. Post-PLA slides were further processed for immunofluorescent staining against the nuclear membrane marker (Lamin A/C, #8617, Cell Signaling). After washing three times with PBST, the slides were mounted with Prolong™ Glass Antifade Mountant with NucBlue™ Stain (#P36985, Thermo Fisher Scientific). The Leica SP8 confocal microscope detected PLA signals as discrete punctate foci and provided the intracellular localization of the complex. ImageJ was used to quantify the nuclear PLA foci.

Crystal Violet Cell Viability assay

In 96-well plates, 5×10^4 cells/well of MDA-MB-231, BT549, SUM159, or SUM1315 cells were transfected with control siRNAs or siRNAs targeting p53, PITPα, PITPβ, PITPNC1, or the combination of PITPα and PITPβ as indicated for 48 h. For the KD rescue experiments, MDA-MB-231 cells were transfected with control siRNAs or siRNAs targeting 3'UTR of PITPα and PITPβ for 24 h. Then the cells were transfected with either HA-tagged wild-type PITPα or its PI-binding deficient T59D mutant PITPα for another 24 h. The cells were then treated with the control vehicle or 30 μM cisplatin for 24 h. Next, the cells were fixed with 4% PFA and stained with 0.2% Crystal Violet. After washing the cells 3 times with PBS, the plates were air-dried at room temperature and imaged using EVOS M5000 Imaging System (ThermoFisher Scientific). After imaging, the dye was extracted from the cells with 10% acetic acid and quantified by measuring the absorbance at 570 nm using a Synergy HTX Multi-Mode Microplate reader.

Caspase-3 Activity Assay

In 6-well plates, 1×10^6 cells/well of MDA-MB-231, BT549, SUM159, or SUM1315 were transfected with control siRNAs or siRNAs targeting p53, PITPα, PITPβ, PITPNC1, or the combination of PITPα and PITPβ as indicated for 48 h. For the KD rescue experiments, MDA-MB-231 cells were transfected with control siRNAs or siRNAs targeting 3'UTR of PITPα and PITPβ for 24 h. Then the cells were transfected with either HA-tagged wild-type PITPα or its PI-binding deficient T59D mutant PITPα for another 24 h. The cells were then treated with the control vehicle or 30 μM cisplatin for 24 h. Next, the cells were lysed and processed for Caspase-3 activity assay by following the manufacturer's instructions

(#E-13183, Thermo Fisher Scientific). At the end of the assay, the fluorescence was read at excitation/emission 342/441 nm using a Synergy HTX Multi-Mode Microplate reader.

Transwell Invasion Assay

The bottom polycarbonate filter surface of a 6.5 mm diameter insert with 8 μm pores in a 24-well plate (#3422, Corning) was coated with 10 μg/ml of Laminin (#CC095, MilliporeSigma) diluted in PBS for 3 h at 37ºC. MDA-MB-231 cells were transiently transfected with control siRNAs or siRNAs targeting the 3'UTR of both PITPα and PITPβ for 24 h. Then the cells were transfected with either HA-tagged wild-type PITPα or its PI-binding deficient T59D mutant PITPα. After 24 h, cells were serum starved for an additional 24 h. Next, $5x10^4$ transfected cells were suspended in 200 μl serum-free medium containing 0.5% BSA and then were plated in the upper insert chamber in 500 μl serum-free medium with 0.5% BSA. 10 ng/ml EGF was added to the lower chamber. Cells were allowed to invade for 16 h at 37°C. Cells on the bottom of the filter were then fixed with 4% PFA and stained with 0.2% Crystal Violet. The stained cells were imaged using EVOS M5000 Imaging System (ThermoFisher Scientific). At the end of the assay, the dye was extracted by 10% acetic acid from the cells and quantified by measuring the optical density at 570 nm using a Synergy HTX Multi-Mode Microplate reader.

Statistics and Reproducibility

Two-tailed unpaired *t*-tests were used for pair-wise significance unless otherwise indicated. We note that no power calculations were used. Sample sizes were determined based on previously published experiments where significant differences were observed

[15, 16]. Each experiment was repeated at least three times independently, and the number of repeats is defined in each figure legend. We used at least three independent experiments or biologically independent samples for statistical analysis.

Resource and Data Availability

All data supporting the findings of this study are available from the corresponding authors on reasonable request.

References

1. Fruman, D.A. *et al.* The PI3K Pathway in Human Disease. *Cell* **170**, 605-635 (2017).
2. Hoxhaj, G. & Manning, B.D. The PI3K-AKT network at the interface of oncogenic signalling and cancer metabolism. *Nat Rev Cancer* **20**, 74-88 (2020).
3. Manning, B.D. & Toker, A. AKT/PKB Signaling: Navigating the Network. *Cell* **169**, 381-405 (2017).
4. Burke, J.E., Triscott, J., Emerling, B.M. & Hammond, G.R.V. Beyond PI3Ks: targeting phosphoinositide kinases in disease. *Nat Rev Drug Discov*, 1-30 (2022).
5. Currie, R.A. *et al.* Role of phosphatidylinositol 3,4,5-trisphosphate in regulating the activity and localization of 3-phosphoinositide-dependent protein kinase-1. *Biochem J* **337 (Pt 3)**, 575-583 (1999).
6. Liu, P. *et al.* PtdIns(3,4,5)P3-Dependent Activation of the mTORC2 Kinase Complex. *Cancer Discov* **5**, 1194-1209 (2015).
7. Calleja, V. *et al.* Intramolecular and intermolecular interactions of protein kinase B define its activation in vivo. *PLoS Biol* **5**, e95 (2007).
8. Altomare, D.A. & Testa, J.R. Perturbations of the AKT signaling pathway in human cancer. *Oncogene* **24**, 7455-7464 (2005).
9. Kondapaka, S.B., Singh, S.S., Dasmahapatra, G.P., Sausville, E.A. & Roy, K.K. Perifosine, a novel alkylphospholipid, inhibits protein kinase B activation. *Mol Cancer Ther* **2**, 1093-1103 (2003).
10. Kikani, C.K. *et al.* Proliferative and antiapoptotic signaling stimulated by nuclear-localized PDK1 results in oncogenesis. *Sci Signal* **5**, ra80 (2012).
11. Shiraishi, I. *et al.* Nuclear targeting of Akt enhances kinase activity and survival of cardiomyocytes. *Circ Res* **94**, 884-891 (2004).
12. Fu, W. & Hall, M.N. Regulation of mTORC2 Signaling. *Genes (Basel)* **11** (2020).
13. Martelli, A.M. *et al.* The emerging multiple roles of nuclear Akt. *Biochim Biophys Acta* **1823**, 2168-2178 (2012).
14. Liu, L. *et al.* DNA-PK promotes activation of the survival kinase AKT in response to DNA damage through an mTORC2-ECT2 pathway. *Sci Signal* **15**, eabh2290 (2022).
15. Chen, M. *et al.* A p53-phosphoinositide signalosome regulates nuclear AKT activation. *Nat Cell Biol* **24**, 1099-1113 (2022).
16. Choi, S., Chen, M., Cryns, V.L. & Anderson, R.A. A nuclear phosphoinositide kinase complex regulates p53. *Nat Cell Biol* **21**, 462-475 (2019).
17. Muller, P.A. & Vousden, K.H. p53 mutations in cancer. *Nat Cell Biol* **15**, 2-8 (2013).
18. Hassin, O. & Oren, M. Drugging p53 in cancer: one protein, many targets. *Nat Rev Drug Discov* **22**, 127-144 (2023).
19. Cocco, L. *et al.* Synthesis of polyphosphoinositides in nuclei of Friend cells. Evidence for polyphosphoinositide metabolism inside the nucleus which changes with cell differentiation. *Biochem J* **248**, 765-770 (1987).
20. Boronenkov, I.V., Loijens, J.C., Umeda, M. & Anderson, R.A. Phosphoinositide signaling pathways in nuclei are associated with nuclear speckles containing pre-mRNA processing factors. *Mol Biol Cell* **9**, 3547-3560 (1998).
21. Chen, M. *et al.* The nuclear phosphoinositide response to stress. *Cell Cycle* **19**, 268-289 (2020).

22. Blind, R.D. *et al.* The signaling phospholipid PIP3 creates a new interaction surface on the nuclear receptor SF-1. *Proc Natl Acad Sci U S A* **111**, 15054-15059 (2014).
23. Hunt, A.N., Clark, G.T., Attard, G.S. & Postle, A.D. Highly saturated endonuclear phosphatidylcholine is synthesized in situ and colocated with CDP-choline pathway enzymes. *J Biol Chem* **276**, 8492-8499 (2001).
24. Wang, Y., Sweitzer, T.D., Weinhold, P.A. & Kent, C. Nuclear localization of soluble CTP:phosphocholine cytidylyltransferase. *J Biol Chem* **268**, 5899-5904 (1993).
25. Tribble, E.K. *et al.* Quantitative profiling of the endonuclear glycerophospholipidome of murine embryonic fibroblasts. *J Lipid Res* **57**, 1492-1506 (2016).
26. Blunsom, N.J. & Cockcroft, S. Phosphatidylinositol synthesis at the endoplasmic reticulum. *Biochim Biophys Acta Mol Cell Biol Lipids* **1865**, 158471 (2020).
27. Bahmanyar, S. Spatial regulation of phospholipid synthesis within the nuclear envelope domain of the endoplasmic reticulum. *Nucleus-Phila* **6**, 102-106 (2015).
28. Huang, Y. *et al.* Global tumor protein p53/p63 interactome: making a case for cisplatin chemoresistance. *Cell Cycle* **11**, 2367-2379 (2012).
29. Ashlin, T.G., Blunsom, N.J. & Cockcroft, S. Courier service for phosphatidylinositol: PITPs deliver on demand. *Biochim Biophys Acta Mol Cell Biol Lipids* **1866**, 158985 (2021).
30. Chen, M., Horn, H.T., Wen, T., Cryns, V.L. & Anderson, R.A. Assessing In Situ Phosphoinositide-Protein Interactions Through Fluorescence Proximity Ligation Assay in Cultured Cells. *Methods Mol Biol* **2251**, 133-142 (2021).
31. Kalasova, I. *et al.* Tools for visualization of phosphoinositides in the cell nucleus. *Histochem Cell Biol* **145**, 485-496 (2016).
32. Posor, Y., Jang, W. & Haucke, V. Phosphoinositides as membrane organizers. *Nat Rev Mol Cell Bio* **23**, 797-816 (2022).
33. Xie, Z., Hur, S.K., Zhao, L., Abrams, C.S. & Bankaitis, V.A. A Golgi Lipid Signaling Pathway Controls Apical Golgi Distribution and Cell Polarity during Neurogenesis. *Dev Cell* **44**, 725-740 e724 (2018).
34. Tilley, S.J. *et al.* Structure-function analysis of human [corrected] phosphatidylinositol transfer protein alpha bound to phosphatidylinositol. *Structure* **12**, 317-326 (2004).
35. Alb, J.G., Jr., Gedvilaite, A., Cartee, R.T., Skinner, H.B. & Bankaitis, V.A. Mutant rat phosphatidylinositol/phosphatidylcholine transfer proteins specifically defective in phosphatidylinositol transfer: implications for the regulation of phospholipid transfer activity. *Proc Natl Acad Sci U S A* **92**, 8826-8830 (1995).
36. Stallings, J.D., Tall, E.G., Pentyala, S. & Rebecchi, M.J. Nuclear translocation of phospholipase C-delta1 is linked to the cell cycle and nuclear phosphatidylinositol 4,5-bisphosphate. *J Biol Chem* **280**, 22060-22069 (2005).
37. Jones, D.R. *et al.* Nuclear PtdIns5P as a transducer of stress signaling: an in vivo role for PIP4Kbeta. *Mol Cell* **23**, 685-695 (2006).
38. Bua, D.J., Martin, G.M., Binda, O. & Gozani, O. Nuclear phosphatidylinositol-5-phosphate regulates ING2 stability at discrete chromatin targets in response to DNA damage. *Sci Rep* **3**, 2137 (2013).
39. Yokogawa, T. *et al.* Evidence that 3 '-phosphorylated polyphosphoinositides are generated at the nuclear surface: use of immunostaining technique with monoclonal antibodies specific for PI 3,4-P-2. *Febs Lett* **473**, 222-226 (2000).

40. Li, W. *et al.* Star-PAP control of BIK expression and apoptosis is regulated by nuclear PIPKIalpha and PKCdelta signaling. *Mol Cell* **45**, 25-37 (2012).
41. Mellman, D.L. *et al.* A PtdIns4,5P2-regulated nuclear poly(A) polymerase controls expression of select mRNAs. *Nature* **451**, 1013-1017 (2008).
42. Tanaka, K. *et al.* Evidence that a phosphatidylinositol 3,4,5-trisphosphate-binding protein can function in nucleus. *Journal of Biological Chemistry* **274**, 3919-3922 (1999).
43. Wang, Y.H. *et al.* DNA damage causes rapid accumulation of phosphoinositides for ATR signaling. *Nat Commun* **8**, 2118 (2017).
44. Wang, Y.H. & Sheetz, M.P. When PIP(2) Meets p53: Nuclear Phosphoinositide Signaling in the DNA Damage Response. *Front Cell Dev Biol* **10**, 903994 (2022).
45. Wang, Y.H. & Sheetz, M.P. Transcription-independent functions of p53 in DNA repair pathway selection. *Bioessays* **45**, e2200122 (2023).
46. Barlow, C.A., Laishram, R.S. & Anderson, R.A. Nuclear phosphoinositides: a signaling enigma wrapped in a compartmental conundrum. *Trends Cell Biol* **20**, 25-35 (2010).
47. Cockcroft, S. & Carvou, N. Biochemical and biological functions of class I phosphatidylinositol transfer proteins. *Biochim Biophys Acta* **1771**, 677-691 (2007).
48. Li, F.L. *et al.* Hippo pathway regulation by phosphatidylinositol transfer protein and phosphoinositides. *Nat Chem Biol* **18**, 1076-1086 (2022).
49. Costes, S.V. *et al.* Automatic and quantitative measurement of protein-protein colocalization in live cells. *Biophys J* **86**, 3993-4003 (2004).
50. Schober, P., Boer, C. & Schwarte, L.A. Correlation Coefficients: Appropriate Use and Interpretation. *Anesth Analg* **126**, 1763-1768 (2018).

FIGURE LEGEND

Figure 1. Stress induces the nuclear localization of PITPs.

a, Domains of PITP class I and II protein family members. PITD, PI transfer domain; FFAT, two phenylalanines in an acidic tract; DDHD, Asp-Asp-His-Asp motif; LNS2, Lipin/Nde1/Smp2 domain.

b-c, Confocal images of IF staining against PITPα/PITPβ/PITPNC1 and PI4,5P_2 in MDA-MB-231 cells treated with vehicle or 30 μM cisplatin for 24 h. The nuclei were counterstained by DAPI. The nuclear levels of PITPs and PI4,5P_2 were quantified by ImageJ (**c**). n=3, 10 cells from each independent experiment. See expanded images in Extended Data Fig. 1a.

d, Quantification of nuclear PITPα/PITPβ levels by IF staining in wild-type and mutant p53 expressing cells, including MCF10A (WT), A549 (WT), HCT116 (WT), BT-549 (R249S), Cal33 (R175H), HS578T (V157F), SUM159 (R158InL), and SUM1315 (C135F). n=3, 10 cells from each independent experiment. See IF images in Extended Data Fig. 2a.

e-f, MDA-MB-231 cells were treated with 30 μM cisplatin, 20 μM erastin, 100 μM tBHQ, 100 μM etoposide, 100 μM hydroxyurea, or vehicle for 24 h. The cells were then processed for IF staining against PITPα or PITPβ and PI4,5P_2. The nuclei were counterstained by DAPI. The nuclear levels of PITPs and PI4,5P_2 were quantified by ImageJ (**f**). n=3, 10 cells from each independent experiment. See expanded images in Extended Data Fig. 2b.

g, Confocal IF of PITPα or PITPβ overlaid with the nuclear envelope marker Lamin A/C in MCF10A, A549, MDA-MB-231, SUM1315, and BT-549 cells treated with vehicle or 30 μM cisplatin for 24 h. The nuclei were counterstained by DAPI.

For all panels, data are represented as mean ± SD, *p* value denotes two-sided paired t-test. Scale bar, 5 μm.

Figure 2. PITPs regulate the nuclear PIP_n pool in response to stress.

a-b, MDA-MB-231 cells were transfected with control siRNAs or siRNAs against PITPα, PITPβ, PITPNC1, or both PITPα and PITPβ. After 24h, cells were treated with 30 μM cisplatin or vehicle for 24 h before being processed for IF staining. The nuclear $PI4,5P_2$ level was quantified by ImageJ (**b**). n=3, 10 cells from each independent experiment. See KD validation in Fig. 5a.

c-d, MDA-MB-231 cells were transfected with control siRNAs or siRNAs against both PITPα and PITPβ. After 24 h, cells were treated with 30 μM cisplatin or vehicle for 24 h before being processed for IF staining against PI4P/$PI3,4,5P_3$ (red) and the shared epitope of PITPα and PITPβ (green). The nuclei were counterstained by DAPI. The nuclear PI4P and PI3,4,5P3 levels were quantified by ImageJ (**d**). n=3, 10 cells from each independent experiment. See KD validation in Fig. 5a.

e-g, A549, BT-549, MCF10A, and SUM1315 cells were transfected with control siRNAs or siRNAs against both PITPα and PITPβ. After 24 h, cells were treated with 30 μM cisplatin or vehicle for 24 h before being processed for IF staining against $PI4,5P_2$ (red) and the shared epitope of PITPα and PITPβ (green). The nuclei were counterstained by DAPI. The nuclear $PI4,5P_2$ levels were quantified by ImageJ (**g**). n=3, 10 cells from each independent experiment. See KD validation in Fig. 2e and expanded images in Extended Data Fig. 3e.

h, Models showing stress-induced nuclear translocation of PITPα/β to regulate nuclear PIP_n puncta.

For all panels, data are represented as mean ± SD, *p* value denotes two-sided paired t-test. Scale bar, 5 µm.

Figure 3. PITPα/β bind p53 and their interaction is regulated by cellular stress

a-b, PLA of p53-PITPα/PITPβ/PITPNC1/PITPNM1/PITPNM2 in MDA-MB-231 cells treated with vehicle or 30 µM cisplatin for 24 h. The nuclear p53-PITP foci were quantified (**b**). n=3, 10 cells from each independent experiment. See PLA of p53-PITPNM1/PITPNM2 images in Extended Data Fig. 4a.

c, PLA of p53-PITPα/PITPβ/PITPNC1 overlaid with the nuclear envelope marker Lamin A/C in MDA-MB-231 cells treated with vehicle or 30 µM cisplatin for 24 h. The nuclei were counterstained by DAPI.

d-g, Co-IP of PITPα/PITPβ/Hsp27 with p53 from MDA-MB-231 cells treated with vehicle or 30 µM cisplatin for 24 h. PITPα IP-ed by p53 (**e**), PITPβ IP-ed by p53 (**f**), and Hsp27 IP-ed by p53 (**g**), as well as PITPNC1/PITPNM1/PITPNM2 were analyzed by WB. n=3 independent experiments.

h-k, Co-IP of p53/Hsp27/ αB-crystallin (αBC) with the shared epitope of PITPα/β from MDA-MB-231 cells treated with vehicle or 30 µM cisplatin for 24 h. p53 IP-ed by PITPα/β (**i**), Hsp27 IP-ed by PITPα/β (**j**), and αBC IP-ed by PITPα/β (**k**) were analyzed by WB. n=3 independent experiments.

l-o, *In vitro* binding of recombinant p53 with PITPα or PITPβ. p53 immobilized on anti-p53 agarose was incubated with PITPα or PITPβ protein. p53 was IP'ed and p53-bound PITPα (**l**,**m**) or PITPβ (**n**,**o**) was analyzed by WB and quantified by ImageJ. n=3 independent experiments.

p, Model showing stress-induced formation of nuclear PITPα/β, p53, and small heat shock protein (sHSP) complexes.

For all panels, data are represented as mean ± SD, *p* value denotes two-sided paired t-test. Scale bar, 5 µm.

Figure 4. PITPα/PITPβ regulate the binding of PIP_ns with p53 in response to stress

a-c, MDA-MB-231 cells were transfected with control siRNAs or siRNAs against p53, PITPα, PITPβ, PITPNC1, or both PITPα and PITPβ. After 24 h, cells were treated with 30 µM cisplatin or vehicle for 24 h before being processed for PLA to detect p53-$PI4,5P_2$/-$PI3,4,5P_3$ complexes (**b,c**). n=3, 10 cells from each independent experiment.

d-f, A549 cells were transfected with control siRNAs or siRNAs against PITPα, PITPβ, or both PITPα and PITPβ. After 24 h, cells were treated with 30 µM cisplatin or vehicle for 24 h before being processed for proximity ligation assay (PLA) to detect p53-$PI4,5P_2$/$PI3,4,5P_3$ complexes (**e,f**). n=3, 10 cells from each independent experiment.

g-j, MDA-MB-231 cells were transfected with control siRNAs or siRNAs against PITPα, PITPβ, or both PITPα and PITPβ. After 24 h, cells were treated with 30 µM cisplatin or vehicle for 24 h before being processed for IP against p53. p53-bound PI4P/$PI4,5P_2$/$PI3,4,5P_3$ were examined by fluorescent WB and quantified by ImageJ (**h-j**)**.** n=3 independent experiments. See KD validation in Fig. 5a.

k-l, A549 cells were transfected with control siRNAs or siRNAs against PITPα, PITPβ, or both PITPα and PITPβ. After 24 h, cells were treated with 30 µM cisplatin or vehicle for 24 h before being processed for IP against p53. The $PI4,5P_2$ level on IP-ed p53 (**l**) was quantified by ImageJ. n=3 independent experiments. See KD validation in Fig. 5b.

For all graphs, data are presented as the mean ± SD, and *p* values are from two-sided paired t-tests. Scale bar, 5 µm.

Figure 5. PITPα/β regulate p53 stability and PIP_n binding to protein targets

a, MDA-MB-231 cells were transfected with control siRNAs or siRNAs against p53, PITPα, PITPβ, PITPNC1, or both PITPα and PITPβ. After 24 h, cells were treated with 30 µM cisplatin or vehicle for 24 h before being processed for WB to validate the KD. The p53 level was quantified by ImageJ. n=3 independent experiments.

b, A549 cells were transfected with control siRNAs or siRNAs against PITPα, PITPβ, or both PITPα and PITPβ. After 24 h, cells were treated with 30 µM cisplatin or vehicle for 24 h before being processed for WB. The p53 level and protein-bound $PI4,5P_2$ level were quantified by ImageJ. n=3 independent experiments.

c-d, MDA-MB-231 cells were transfected with control siRNAs or siRNAs against p53, PITPα, PITPβ, PITPNC1, or both PITPα and PITPβ. After 24 h, cells were treated with 30 µM cisplatin or vehicle for 24 h before being processed for triple fluorescent WB for detecting p53 (Red), GAPDH (Blue), and protein-bound $PI4,5P_2$ (Green) simultaneously. The protein-bound $PI4,5P_2$ levels were quantified by ImageJ (**d**). See KD validation in Fig. 5a. n=3 independent experiments.

e-f, A549 cells were transfected with control siRNAs or siRNAs against PITPα or PITPβ. After 24 h, cells were treated with 30 µM cisplatin or vehicle for 24 h before being processed for WB. The protein-bound PIP_n levels were quantified by ImageJ (**f**). n=3 independent experiments.

g, Model showing the nuclear p53-PIP_n signalosome downstream of PITPα/β.

For all graphs, data are presented as the mean ± SD, and *p* values are from two-sided paired t-tests.

Figure 6. PITPα/β regulate p53-dependent nuclear Akt activation and cell survival

a-b, MDA-MB-231 cells were transfected with control siRNAs or siRNAs against PITPα, PITPβ, PITPNC1, or both PITPα and PITPβ. After 24h, cells were treated with 30 μM cisplatin or vehicle for 24 h before being processed for IF staining against $pAkt^{S473}$. The nuclear $pAkt^{S473}$ levels were quantified by ImageJ (**b**). n=3, 10 cells from each independent experiment. Scale bar, 5 μm.

c-e, BT-549, SUM159, and SUM1315 cells with the indicated p53 status were transfected with control siRNAs or siRNAs against both PITPα and PITPβ. After 24 h, cells were treated with 30 μM cisplatin or vehicle for 24 h before being processed for IF staining against $PI4,5P_2$. The nuclei were counterstained by DAPI. The nuclear $PI4,5P_2$ levels were quantified (**d**). n=3, 10 cells from each independent experiment. Scale bar, 5 μm. The double KD of PITPα and PITPβ in SUM159 cells was validated by WB (**e**). See KD validation for BT-549 and SUM1315 cells in Fig. 2e.

f-g, MDA-MB-231 cells were transfected with control siRNAs or siRNAs against p53, PITPα, PITPβ, PITPNC1, or both PITPα and PITPβ. After 24h, cells were treated with 30 μM cisplatin or vehicle for 24 h before being processed for Crystal Violet viability assay. The cells were imaged by EVOS M5000 microscope (**f**) and quantified based on the extracted dye using a plate reader (**g**). Scale bar, 300 μm.

h, MDA-MB-231 cells were transfected with control siRNAs or siRNAs against p53, PITPα, PITPβ, PITPNC1, or both PITPα and PITPβ. After 24h, cells were treated with 30 μM

cisplatin or vehicle for 24 h before being processed for caspase 3 activity assay. n=3 independent experiments.

For all graphs, data are presented as the mean ± SD, and *p* values are from two-sided paired t-tests.

Figure 7. PITPα/β initiate the p53-PIP_n signalosome by a PI binding-dependent mechanism

a, HEK293FT cells were co-transfected with either HA-tagged wild-type PITPα or PI binding-defective mutant T59D PITPα together with Flag-tagged $p53^{wt}$. After 48 h, cells were processed for IP against Flag-tag and analyzed by WB. n=3 independent experiments.

b-e, MDA-MB-231 cells were transfected with control siRNAs or siRNAs against the 3'UTR of both PITPα and PITPβ for 24 h. Then the cells were transfected with either HA-tagged wild-type PITPα/β or PI binding-defective mutant T59D PITPα. After 24 h, cells were treated with 30 μM cisplatin or vehicle for 24 h before being processed for WB (**b**) and IF staining against HA-tag with $PI4,5P_2$ or $pAkt^{S473}$ (**c**). The nuclear $PI4,5P_2$ and $pAkt^{S473}$ levels in HA-positive cells were quantified by ImageJ (**d, e**). n=3, 10 cells from each independent experiment. Scale bar, 5 μm.

f-i, Pearson's correlation coefficient (Pearson's r) quantified the correlations between nuclear $PI4,5P_2$ or $pAkt^{S473}$ with HA-$PITPα^{wt/T59D}$ levels. n=100 cells pooled from 3 independent experiments.

j-k, MDA-MB-231 cells were transfected with control siRNAs or siRNAs against the 3'UTR of both PITPα and PITPβ for 24 h. The cells were then transfected with either HA-tagged

wild-type PITPα or PI binding-defective mutant T59D PITPα. After 24 h, cells were treated with 30 µM cisplatin or vehicle for 24 h before being processed for Crystal Violet viability assay. The cells were imaged by EVOS M5000 microscope (**j**) and quantified based on the extracted dye using a plate reader (**k**). n=3 independent experiments. Scale bar, 300 µm.

l-m, MDA-MB-231 cells were transfected with control siRNAs or siRNAs against the 3'UTR of both PITPα and PITPβ for 24 h. The cells were then transfected with either HA-tagged wild-type PITPα or PI binding-defective mutant T59D PITPα. After 24 h, cells were serum starved for an additional 24 h and then scored for invasion through Laminin-coated transwell inserts with 8 µm pores using 10 ng/ml EGF as a chemoattractant for 16 h. The invading cells at the insert bottom were stained with Crystal Violet, imaged (**l**), and quantified (**m**) based on the extracted dye using a plate reader. n=3 independent experiments. Scale bar, 300 µm.

n, A model of the stress-induced nuclear accumulation of PITPs and PITP-dependent initiation of the p53-PI signalosome which promotes cell proliferation, survival, and invasion.

For all graphs, data are presented as the mean ± SD, and *p* values are from two-sided paired t-tests.

SUPLEMENTAL INFORMATION

Extended Data Figure 1. Cisplatin induces the nuclear accumulation of PITPs

a, Confocal images of IF staining against PITPα/PITPβ/PITPNC1 and PI4,5P_2 in MDA-MB-231 cells treated with vehicle or 30 µM cisplatin for 24 h. The nuclei were counterstained by DAPI. See quantification in Fig. 1c.

b-c, 3D sections of IF staining against PITPα in MDA-MB-231 cells treated with vehicle or 30 μM cisplatin for 24 h. The nuclei were counterstained by DAPI. Each frame of the 3D sections was over a 0.2 μm thickness.

d-e, 3D sections of IF staining against PITPβ in MDA-MB-231 cells treated with vehicle or 30 μM cisplatin for 24 h. The nuclei were counterstained by DAPI. Each frame of the 3D sections was over a 0.2 μm thickness.

For all panels, Scale bar, 5 μm.

Extended Data Figure 2. Diverse cellular stressors induce the nuclear localization of PITPs in multiple cell lines

a, Confocal images of the IF staining against PITPα/β in wild-type and mutant p53 expressing cells, including MCF10A (WT), A549 (WT), HCT116 (WT), BT-549 (R249S), Cal33 (R175H), HS578T (V157F), SUM159 (R158InL), and SUM1315 (C135F). The nuclei were counterstained by DAPI. See the quantification of the nuclear levels of PITPα/PITPβ in Fig. 1d.

b, MDA-MB-231 cells treated with 30 μM cisplatin, 20 μM erastin, 100 μM tBHQ, 100 μM etoposide, 100 μM hydroxyurea, or vehicle for 24 h. The cells were processed for IF staining against PITPα and PI4,5P_2. The nuclei were counterstained by DAPI. See the quantification of nuclear PITPα, PITPβ and PI4,5P_2 in Fig. 1f.

c, Confocal IF of PITPNC1 overlaid with the nuclear envelope marker Lamin A/C in MDAMB-231 and A549 cells treated with vehicle or 30 μM cisplatin for 24 h. The nuclei were counterstained by DAPI.

For all panels, Scale bar, 5 μm.

Extended Data Figure 3. PITPs regulate the non-membranous PI4,5P_2 pools in the nucleus

a-d, Confocal IF images of PITPα/β overlaid with the nuclear envelope marker Lamin A/C in wild-type and mutant p53 expressing cancer cells, including HCT116 (WT, **a**), Cal33 (R175H, **b**), HS578T (V157F, **c**), and SUM159 (R158InL, **d**). The nuclei were counterstained by DAPI.

e, MCF10A and SUM1315 cells with the indicated p53 status were transfected with control siRNAs or siRNAs against both PITPα and PITPβ. After 24 h, cells were treated with 30 μM cisplatin or vehicle for 24 h before being processed for IF staining against PI4,5P_2 (red) and the shared epitope of PITPα and PITPβ (green). The nuclei were counterstained by DAPI. See KD validation in Fig. 2e and quantification in Fig. 2g. n=3, 10 cells from each independent experiment.

For all panels, Scale bar, 5 μm.

Extended Data Figure 4. Stress induces PITPα/β association with p53 in the non-membranous nucleoplasm

a, PLA of p53-PITPNM1/PITPNM2 in MDA-MB-231 cells treated with vehicle or 30 μM cisplatin for 24 h. See quantification in Fig. 3b.

b-c, PLA of p53-PITPα/PITPβ/PITPNC1/PITPNM1/PITPNM2 in A549 cells treated with vehicle or 30 μM cisplatin for 24 h. The nuclear p53-PITP PLA foci were quantified by ImageJ (**c**). n=3, 10 cells from each independent experiment.

d, PLA of p53-PITPα/PITPβ/PITPNC1/PITPNM1/PITPNM2 overlaid with the nuclear envelope marker Lamin A/C in A549 cells treated with vehicle or 30 μM cisplatin for 24 h. The nuclei were counterstained by DAPI.

e, PLA of p53-PITPNM1/PITPNM2 overlaid with the nuclear envelope marker Lamin A/C in MDA-MB-231 treated with vehicle or 30 μM cisplatin for 24 h. The nuclei were counterstained by DAPI.

f, 3D sections of p53-PITPβ PLA foci overlaid with Lamin A/C in MDA-MB-231 treated with vehicle or 30 μM cisplatin for 24 h. The nuclei were counterstained by DAPI. Each frame of the 3D sections was over a 0.2 μm thickness.

For all panels, data are represented as mean ± SD, *p* value denotes two-sided paired t-test. Scale bar, 5 μm unless otherwise indicated.

Extended Data Figure 5. Stress induces PITPα/β association with p53

a-d, Co-IP of p53/Hsp27/αB-crystallin (αBC) with the shared epitope of PITPα/β in MCF10A cells treated with vehicle or 30 μM cisplatin for 24 h. p53 IP-ed by PITPα/β (**b**), Hsp27 IP-ed by PITPα/β (**c**), and αBC IP-ed by PITPα/β (**d**) were analyzed by WB. n=3 independent experiments.

e-f, Co-IP of p53 with the shared epitope of PITPα/β in A549 cells treated with vehicle or 30 μM cisplatin for 24 h. p53 IP-ed by PITPα/β was analyzed by WB (**f**). n=3 independent experiments.

g-h, Co-IP of p53 with the shared epitope of PITPα/β in HCT116 cells treated with vehicle or 30 μM cisplatin for 24 h. p53 IP-ed by PITPα/β was analyzed by WB (**h**). n=3 independent experiments.

i-n, Co-IP of PITPα/PITPβ with p53 in BT549, Cal33, HS578T, SUM159, SUM1315 cells treated with vehicle or 30 μM cisplatin for 24 h. PITPα/PITPβ IP-ed by p53 (**n**) as well as PITPNC1/PITPNM1/PITPNM2 were analyzed by WB. n=3 independent experiments.

For all panels, data are represented as mean ± SD, *p* value denotes two-sided paired t-test.

Extended Data Figure 6. PITPα/β and mutant p53 inhibit genotoxic stress-induced apoptosis

a-g, BT-549, SUM159, and SUM1315 cells were transfected with control siRNAs or siRNAs against p53, PITPα, PITPβ, or both PITPα and PITPβ. After 24 h, cells were treated with 30 μM cisplatin or vehicle for 24 h before being processed for Crystal Violet viability assay. The cells were imaged by EVOS M5000 microscope (**a**) and quantified based on the extracted dye using a plate reader (**b-d**). The KD was validated by WB (**e-g**). n=3 independent experiments.

h-j, BT-549, SUM159, and SUM1315 cells were transfected with control siRNAs or siRNAs against p53, PITPα, PITPβ, or both PITPα and PITPβ. After 24 h, cells were treated with 30 μM cisplatin or vehicle for 24 h before being processed for caspase 3 activity assay. n=3 independent experiments.

For all graphs, data are presented as the mean ± SD, and *p* values are from two-sided paired t-tests. Scale bar, 300 μm.

Extended Data Figure 7. PITPα/β interact with p53 and promote cell survival and invasion by a PI binding-dependent mechanism

a, HEK293FT cells were co-transfected with either HA-tagged wild-type PITPα or PI binding-defective mutant T59D PITPα together with Flag-tagged mutant $p53^{R175H}$. After 48 h, cells were processed for IP against Flag-tag and analyzed by WB. n=3 independent experiments.

b, HEK293FT cells were co-transfected with either HA-tagged wild-type PITPβ or PI binding-defective mutant T59D PITPα together with Flag-tagged $p53^{wt}$. After 48 h, cells were processed for IP against Flag-tag and analyzed by WB. n=3 independent experiments.

c, HEK293FT cells were co-transfected with either HA-tagged wild-type PITPβ or PI binding-defective mutant T59D PITPα together with Flag-tagged mutant $p53^{R175H}$. After 48 h, cells were processed for IP against Flag-tag and analyzed by WB. n=3 independent experiments.

d, MDA-MB-231 cells were transfected with control siRNAs or siRNAs against the 3'UTR of both PITPα and PITPβ for 24 h. The cells were then transfected with either HA-tagged wild-type PITPα or PI binding-defective mutant T59D PITPα. After 24 h, cells were treated with 30 μM cisplatin or vehicle for 24 h before being processed for caspase 3 activity assay. n=3 independent experiments.

For all graphs, data are presented as the mean ± SD, and *p* values are from two-sided paired t-tests. Scale bar, 300 μm.

Fig. 1

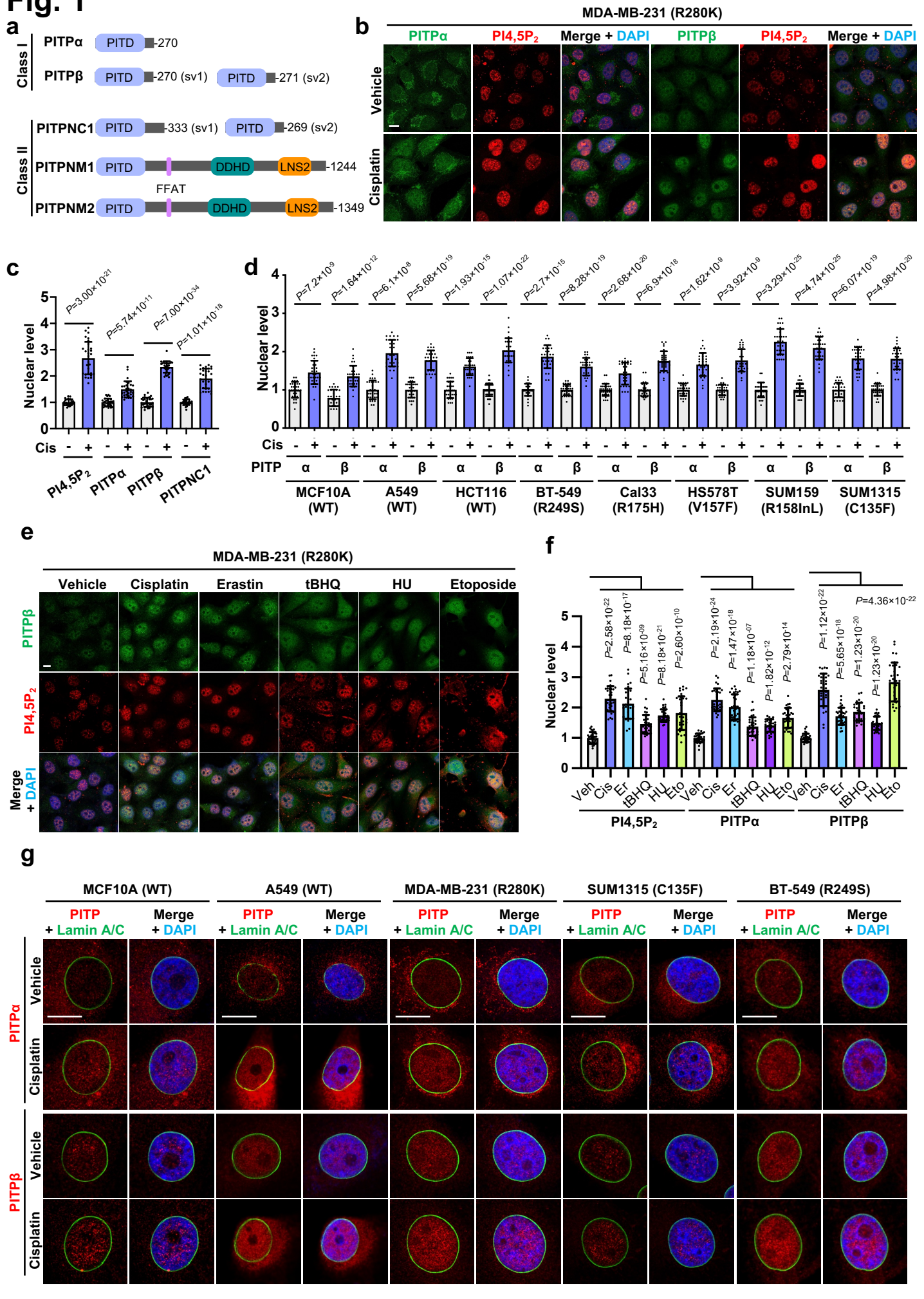
a
Class I
PITPα
PITD
-270
PITPβ
PITD
-270 (sv1)
PITD
-271 (sv2)
Class II
PITPNC1
PITD
-333 (sv1)
PITD
-269 (sv2)
PITPNM1
PITD
DDHD
LNS2
-1244
FFAT
PITPNM2
PITD
DDHD
LNS2
-1349
b
MDA-MB-231 (R280K)
PITPα
PI4,5P2
Merge + DAPI
PITPβ
PI4,5P2
Merge + DAPI
Vehicle
Cisplatin
c
Nuclear level
P=3.00×10-21
P=5.74×10-11
P=7.00×10-34
P=1.01×10-18
Cis
PI4,5P2
PITPα
PITPβ
PITPNC1
d
Nuclear level
P=7.2×10-9
P=1.64×10-12
P=6.1×10-8
P=5.68×10-19
P=1.93×10-15
P=1.07×10-22
P=2.7×10-15
P=8.28×10-19
P=2.68×10-20
P=6.9×10-18
P=1.62×10-9
P=3.92×10-9
P=3.29×10-25
P=4.74×10-25
P=6.07×10-19
P=4.98×10-20
Cis
PITP
MCF10A (WT)
A549 (WT)
HCT116 (WT)
BT-549 (R249S)
Cal33 (R175H)
HS578T (V157F)
SUM159 (R158InL)
SUM1315 (C135F)
e
MDA-MB-231 (R280K)
Vehicle
Cisplatin
Erastin
tBHQ
HU
Etoposide
PITPβ
PI4,5P2
Merge + DAPI
f
Nuclear level
P=2.58×10-22
P=8.18×10-17
P=5.16×10-09
P=8.18×10-21
P=2.60×10-10
P=2.19×10-24
P=1.47×10-18
P=1.18×10-07
P=1.82×10-12
P=2.79×10-14
P=1.12×10-22
P=5.65×10-18
P=1.23×10-20
P=1.23×10-20
P=4.36×10-22
Veh
Cis
Er
tBHQ
HU
Eto
PI4,5P2
PITPα
PITPβ
g
MCF10A (WT)
A549 (WT)
MDA-MB-231 (R280K)
SUM1315 (C135F)
BT-549 (R249S)
PITP + Lamin A/C
Merge + DAPI
PITPα
PITPβ
Vehicle
Cisplatin

Extended Data Fig. 1

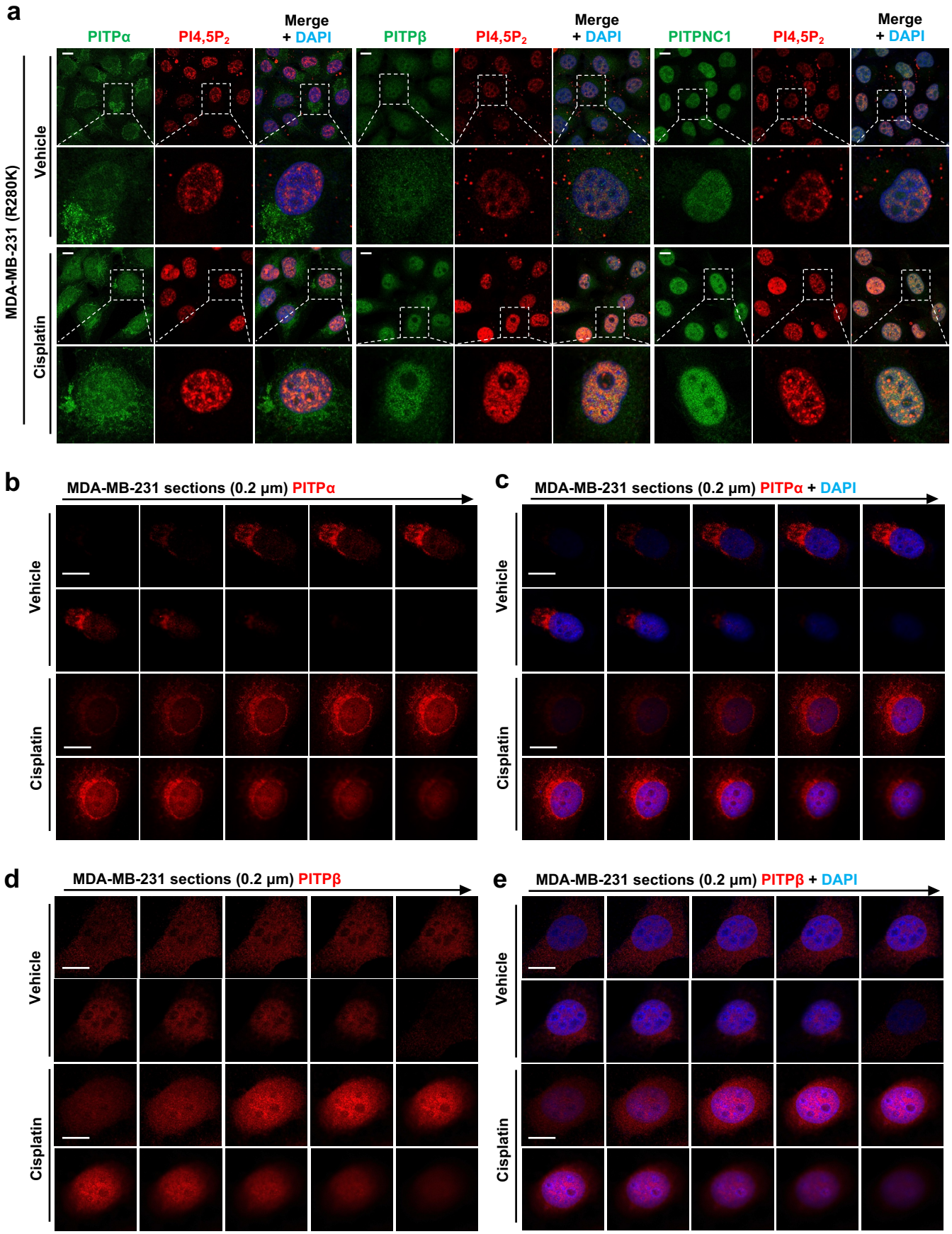

Extended Data Fig. 2

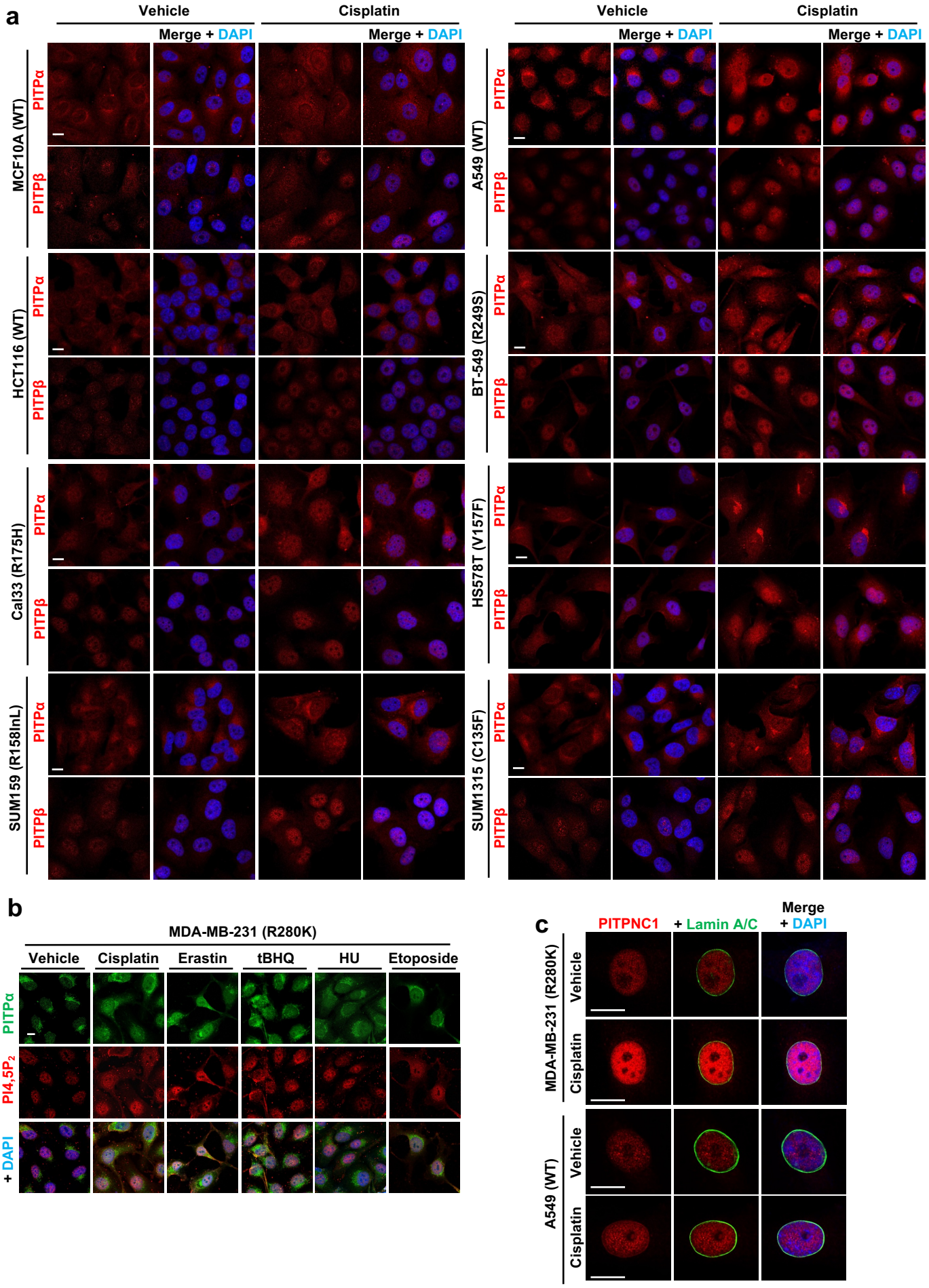

Extended Data Fig. 3

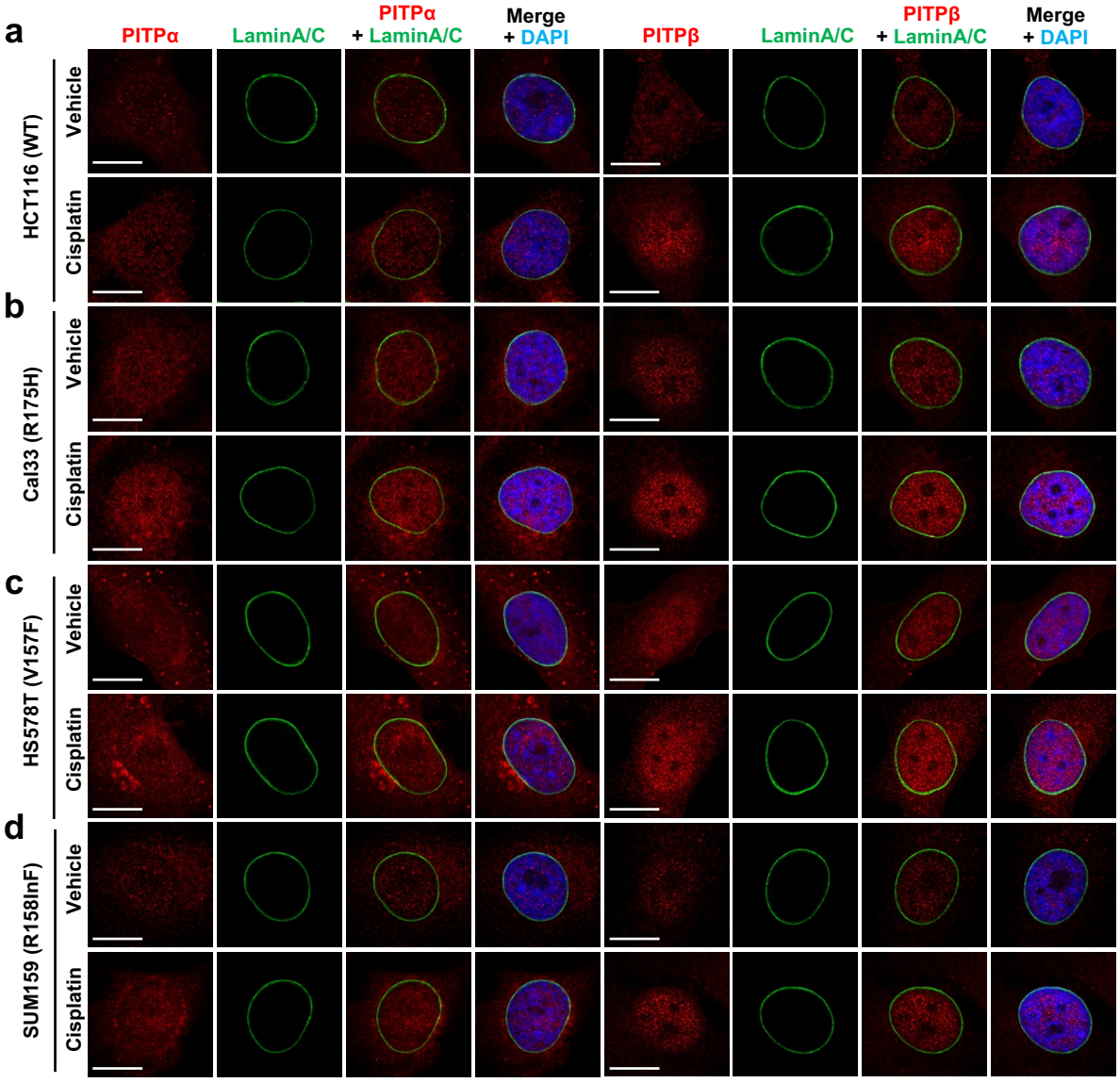

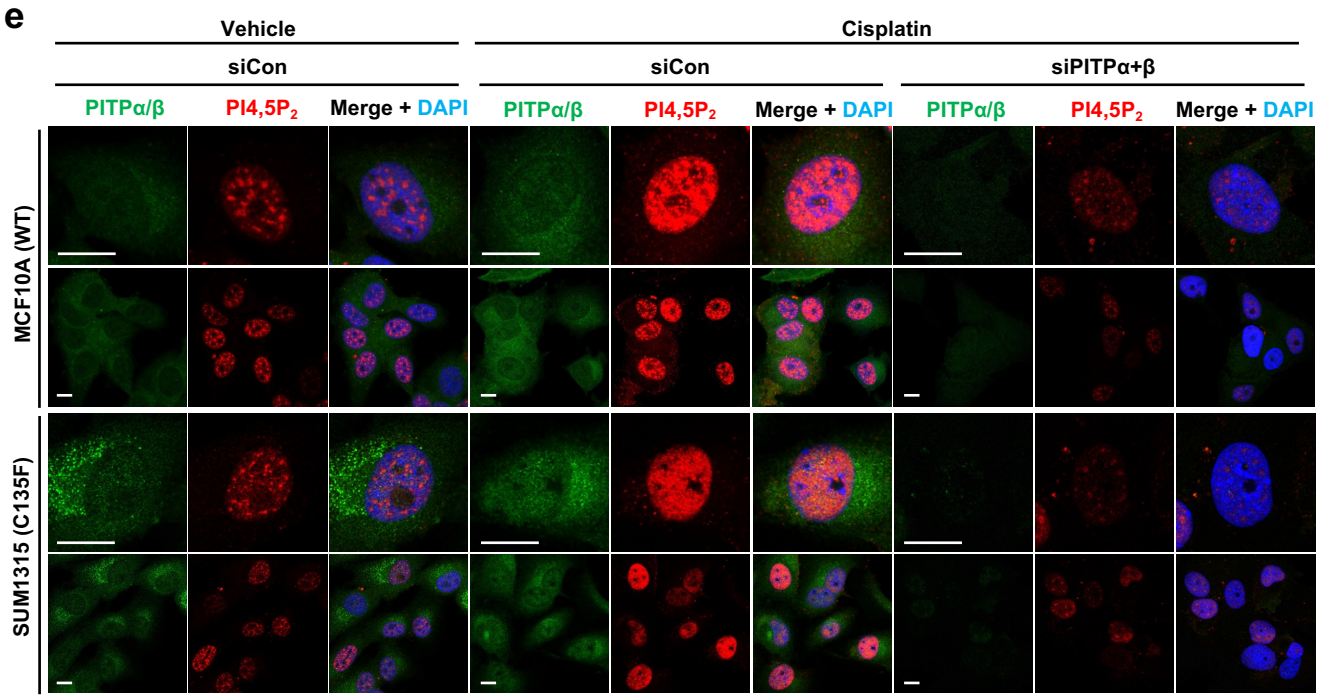

Fig. 2

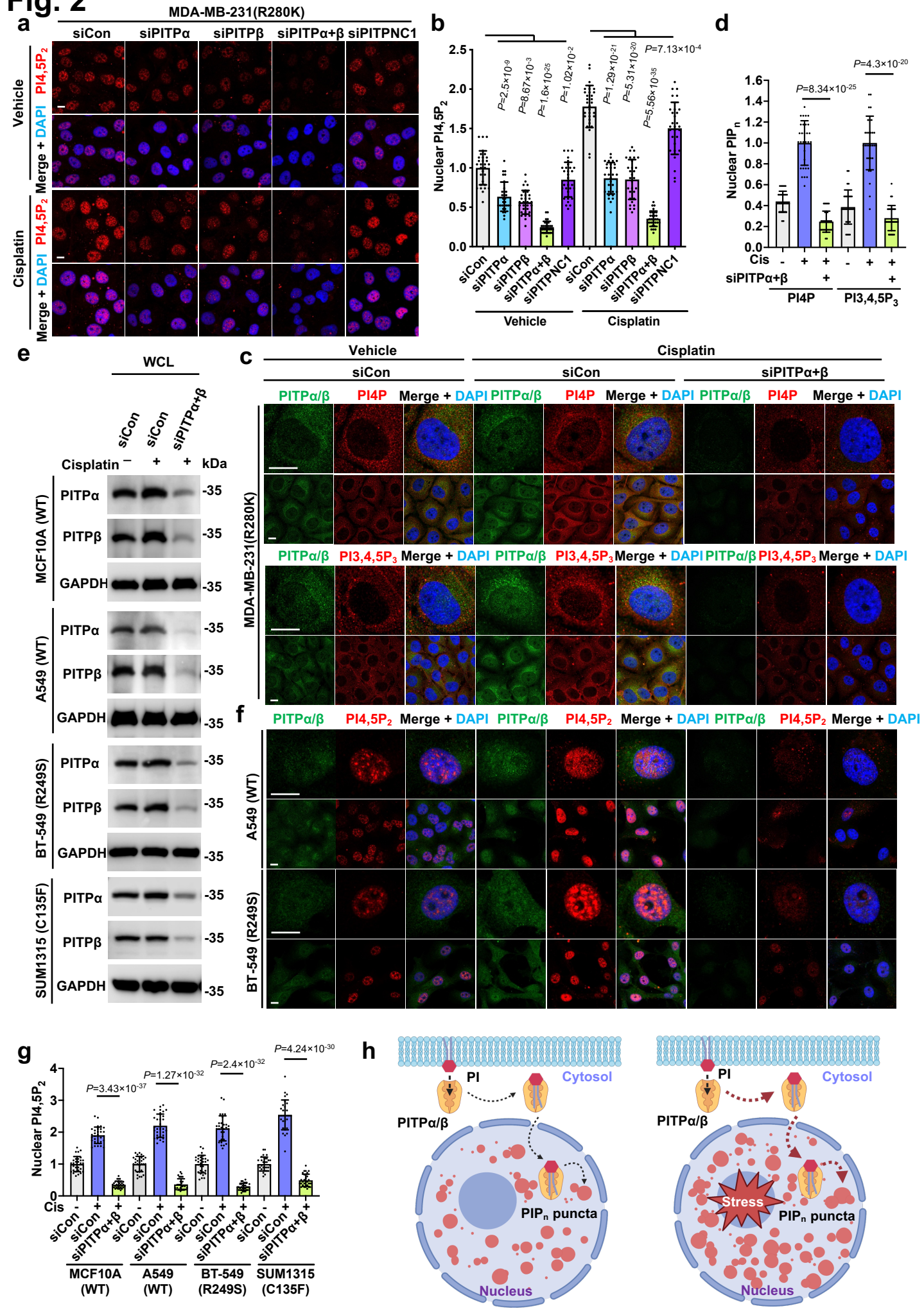
a
MDA-MB-231(R280K)
siCon
siPITPα
siPITPβ
siPITPα+β
siPITPNC1
Vehicle
Cisplatin
PI4,5P2
Merge + DAPI
b
Nuclear PI4,5P2
P=2.5×10-9
P=8.67×10-3
P=1.6×10-25
P=1.02×10-2
P=1.29×10-21
P=5.31×10-20
P=5.56×10-35
P=7.13×10-4
siCon
siPITPα
siPITPβ
siPITPα+β
siPITPNC1
Vehicle
Cisplatin
d
Nuclear PIPn
P=8.34×10-25
P=4.3×10-20
Cis
siPITPα+β
PI4P
PI3,4,5P3
e
WCL
siCon
siCon
siPITPα+β
Cisplatin
kDa
MCF10A (WT)
A549 (WT)
BT-549 (R249S)
SUM1315 (C135F)
PITPα
PITPβ
GAPDH
-35
c
Vehicle
Cisplatin
siCon
siCon
siPITPα+β
PITPα/β
PI4P
Merge + DAPI
PI3,4,5P3
MDA-MB-231(R280K)
f
PI4,5P2
A549 (WT)
BT-549 (R249S)
g
Nuclear PI4,5P2
P=3.43×10-37
P=1.27×10-32
P=2.4×10-32
P=4.24×10-30
Cis
siCon
siPITPα+β
MCF10A (WT)
A549 (WT)
BT-549 (R249S)
SUM1315 (C135F)
h
PI
Cytosol
PITPα/β
PIPn puncta
Nucleus
Stress

Fig. 3

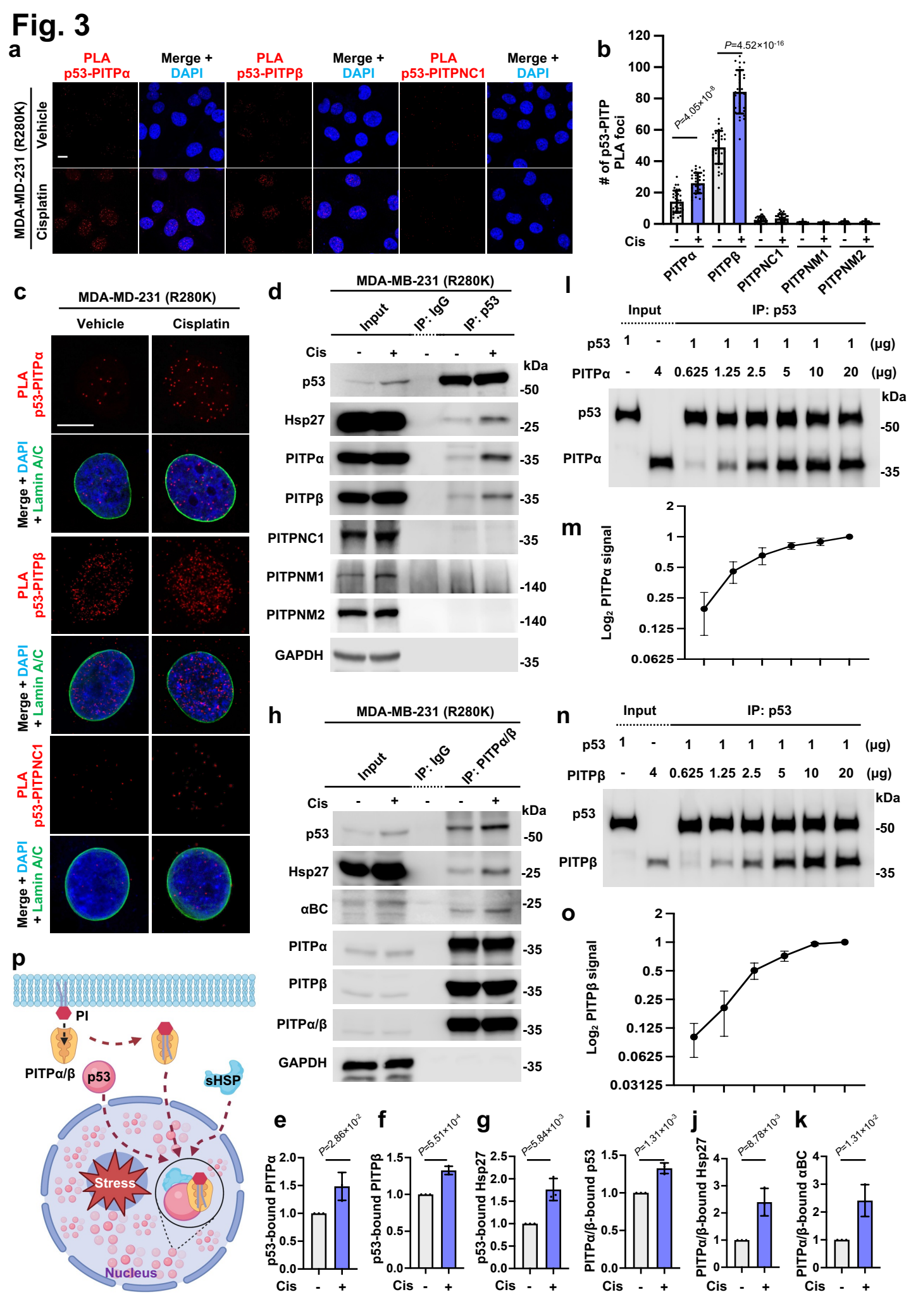
a
PLA p53-PITPα
Merge + DAPI
PLA p53-PITPβ
Merge + DAPI
PLA p53-PITPNC1
Merge + DAPI
MDA-MD-231 (R280K)
Vehicle
Cisplatin
b
# of p53-PITP PLA foci
P=4.05×10-8
P=4.52×10-16
Cis
PITPα
PITPβ
PITPNC1
PITPNM1
PITPNM2
c
MDA-MD-231 (R280K)
Vehicle
Cisplatin
PLA p53-PITPα
Merge + DAPI + Lamin A/C
PLA p53-PITPβ
Merge + DAPI + Lamin A/C
PLA p53-PITPNC1
Merge + DAPI + Lamin A/C
d
MDA-MB-231 (R280K)
Input
IP: IgG
IP: p53
Cis
kDa
p53
Hsp27
PITPα
PITPβ
PITPNC1
PITPNM1
PITPNM2
GAPDH
l
Input
IP: p53
p53
PITPα
(μg)
m
Log2 PITPα signal
h
MDA-MB-231 (R280K)
Input
IP: IgG
IP: PITPα/β
Cis
kDa
p53
Hsp27
αBC
PITPα
PITPβ
PITPα/β
GAPDH
n
Input
IP: p53
p53
PITPβ
(μg)
o
Log2 PITPβ signal
p
PI
PITPα/β
p53
sHSP
Stress
Nucleus
e
p53-bound PITPα
P=2.86×10-2
f
p53-bound PITPβ
P=5.51×10-4
g
p53-bound Hsp27
P=5.84×10-3
i
PITPα/β-bound p53
P=1.31×10-3
j
PITPα/β-bound Hsp27
P=8.78×10-3
k
PITPα/β-bound αBC
P=1.31×10-2
Cis

Extended Data Fig. 4

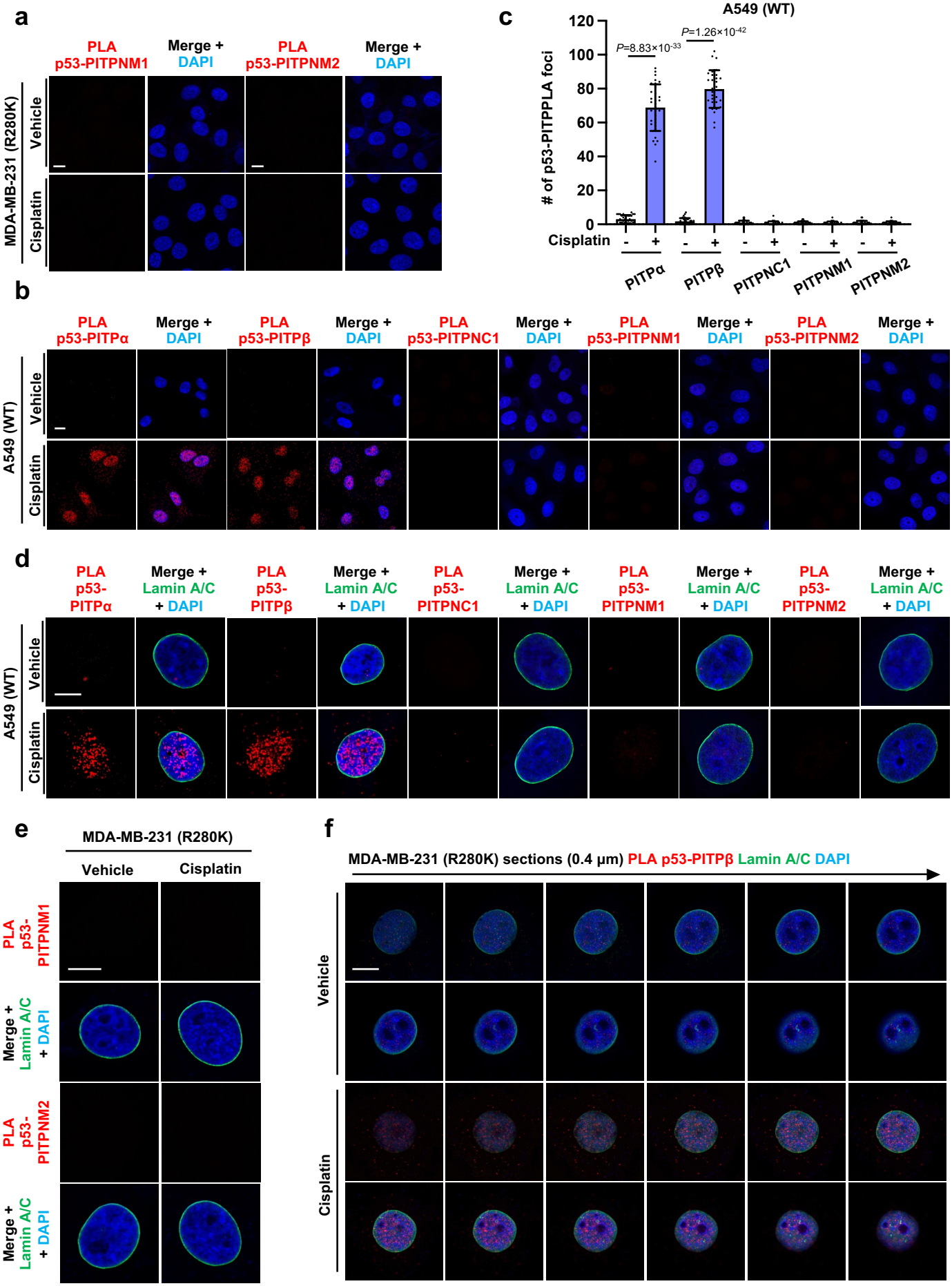

Extended Data Fig. 5

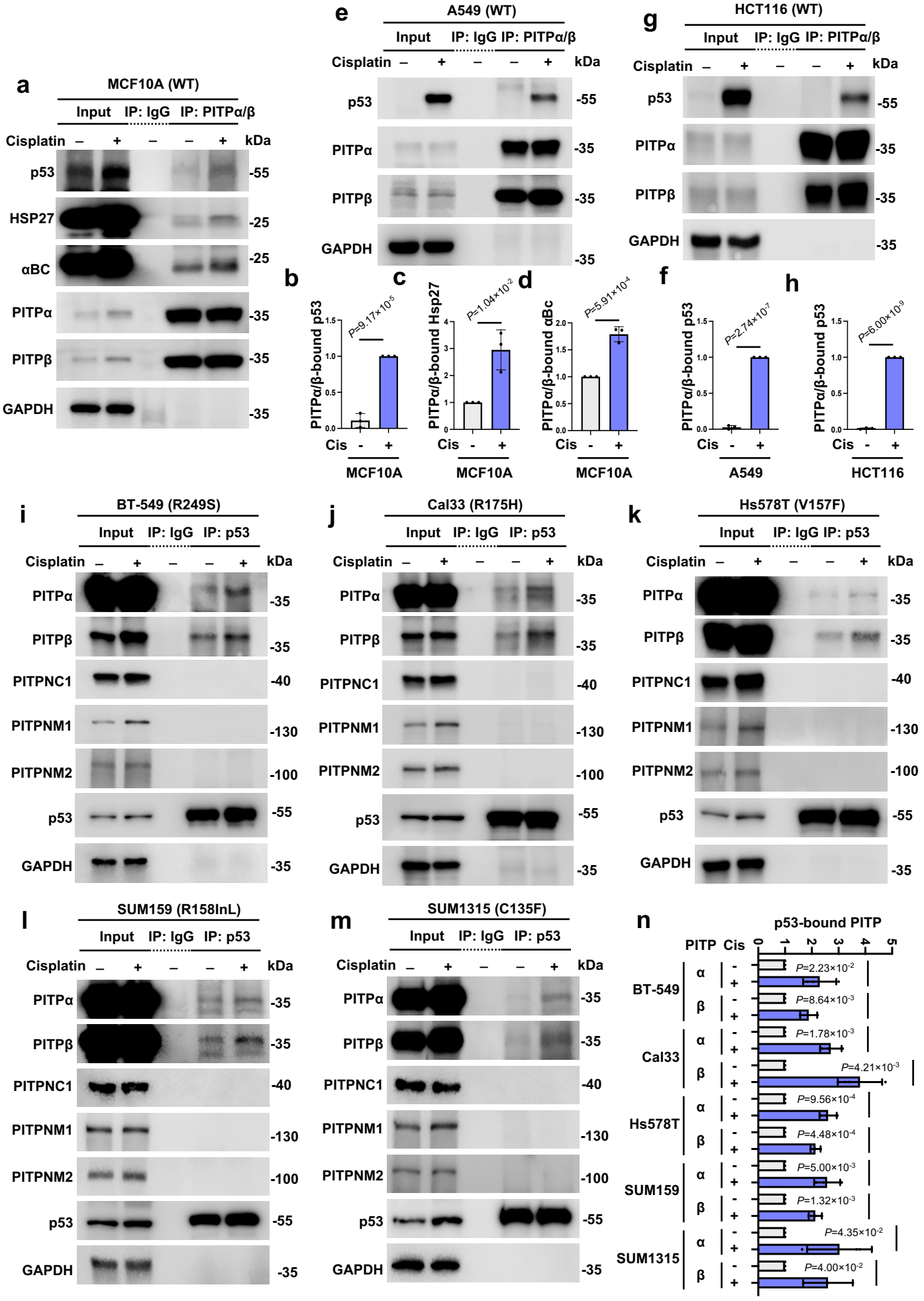

Fig. 4

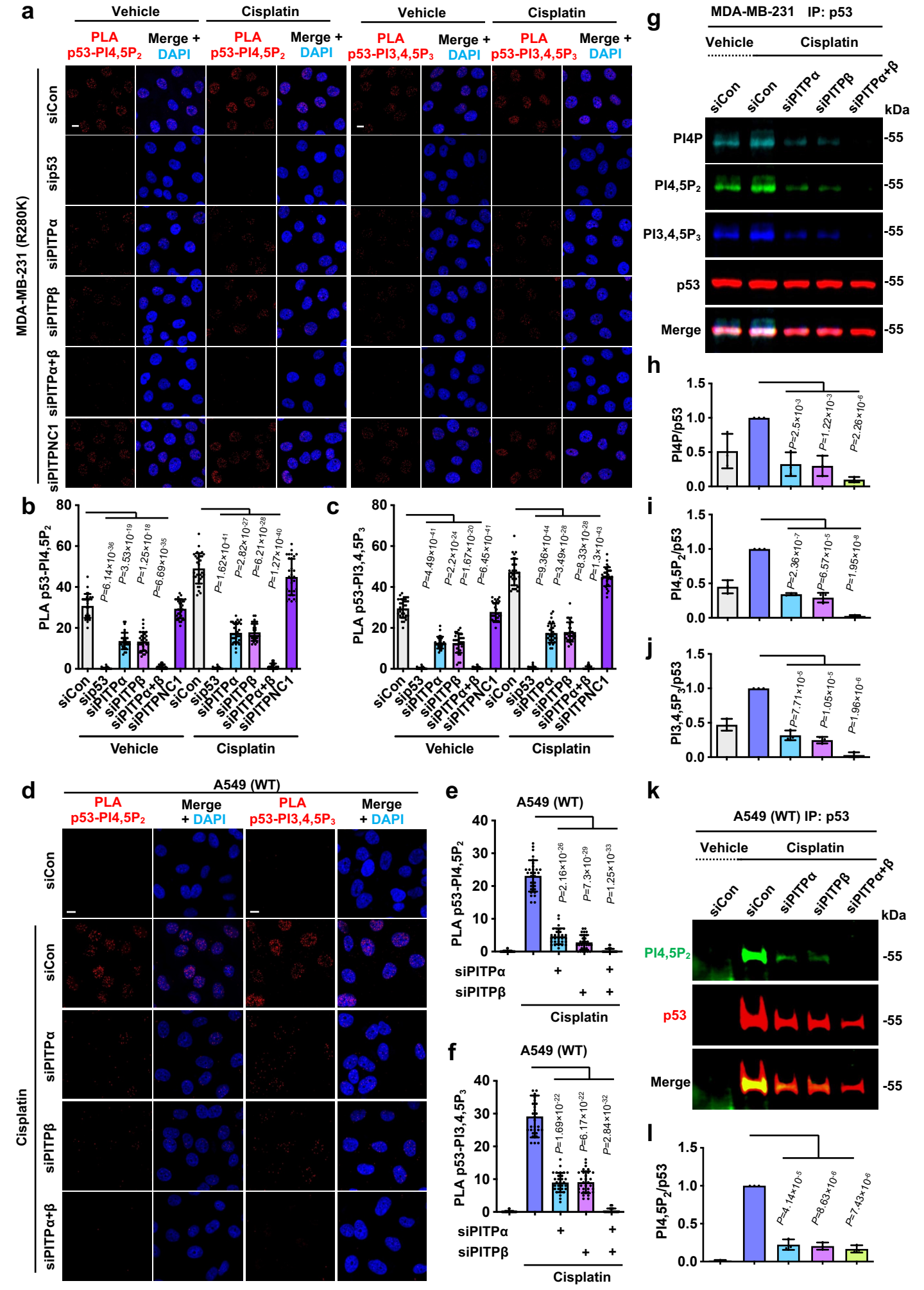
a
Vehicle
Cisplatin
Vehicle
Cisplatin
PLA p53-PI4,5P2
Merge + DAPI
PLA p53-PI3,4,5P3
Merge + DAPI
MDA-MB-231 (R280K)
siCon
sip53
siPITPα
siPITPβ
siPITPα+β
siPITPNC1
b
PLA p53-PI4,5P2
P=6.14×10-36
P=3.53×10-19
P=1.25×10-18
P=6.69×10-35
P=1.62×10-41
P=2.82×10-27
P=6.21×10-28
P=1.27×10-40
c
PLA p53-PI3,4,5P3
P=4.49×10-41
P=2.2×10-24
P=1.67×10-20
P=6.45×10-41
P=9.36×10-44
P=3.49×10-28
P=8.33×10-28
P=1.3×10-43
Vehicle
Cisplatin
g
MDA-MB-231 IP: p53
Vehicle
Cisplatin
siCon
siCon
siPITPα
siPITPβ
siPITPα+β
kDa
PI4P
PI4,5P2
PI3,4,5P3
p53
Merge
-55
h
PI4P/p53
P=2.5×10-3
P=1.22×10-3
P=2.26×10-6
i
PI4,5P2/p53
P=2.36×10-7
P=6.57×10-5
P=1.95×10-8
j
PI3,4,5P3/p53
P=7.71×10-5
P=1.05×10-5
P=1.96×10-6
d
A549 (WT)
PLA p53-PI4,5P2
Merge + DAPI
PLA p53-PI3,4,5P3
Merge + DAPI
siCon
Cisplatin
siPITPα
siPITPβ
siPITPα+β
e
A549 (WT)
PLA p53-PI4,5P2
P=2.16×10-26
P=7.3×10-29
P=1.25×10-33
siPITPα
siPITPβ
Cisplatin
f
A549 (WT)
PLA p53-PI3,4,5P3
P=1.69×10-22
P=6.17×10-22
P=2.84×10-32
siPITPα
siPITPβ
Cisplatin
k
A549 (WT) IP: p53
Vehicle
Cisplatin
siCon
siCon
siPITPα
siPITPβ
siPITPα+β
kDa
PI4,5P2
p53
Merge
-55
l
PI4,5P2/p53
P=4.14×10-5
P=8.63×10-6
P=7.43×10-6

Fig. 5

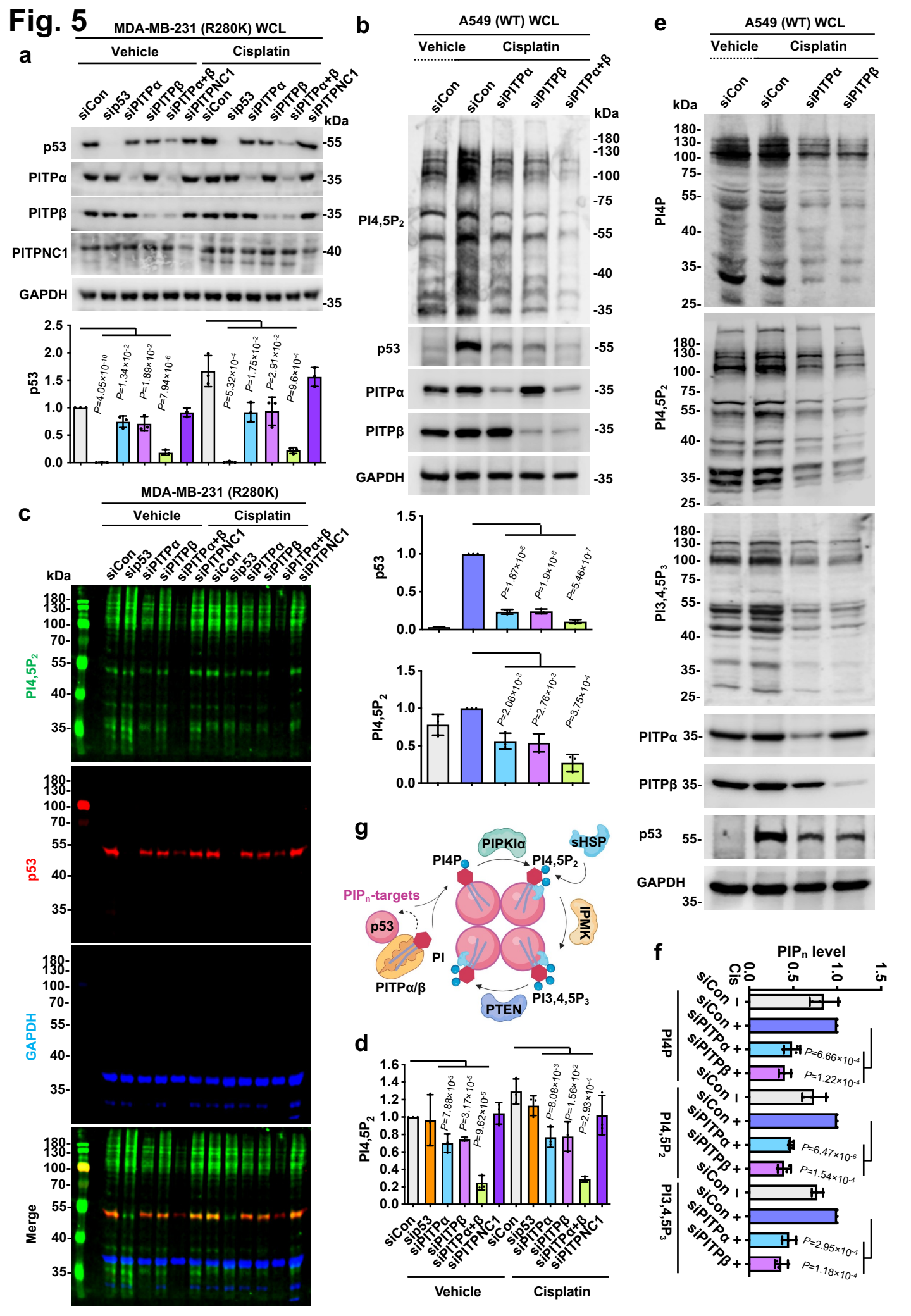
a
MDA-MB-231 (R280K) WCL
Vehicle
Cisplatin
siCon
sip53
siPITPα
siPITPβ
siPITPα+β
siPITPNC1
kDa
p53
PITPα
PITPβ
PITPNC1
GAPDH
-55
-35
-35
-40
-35
P=4.05×10-10
P=1.34×10-2
P=1.89×10-2
P=7.94×10-6
P=5.32×10-4
P=1.75×10-2
P=2.91×10-2
P=9.6×10-4
b
A549 (WT) WCL
PI4,5P2
-180
-130
-100
-75
-55
-40
-35
P=1.87×10-6
P=1.9×10-6
P=5.46×10-7
P=2.06×10-3
P=2.76×10-3
P=3.75×10-4
c
MDA-MB-231 (R280K)
PI4,5P2
p53
GAPDH
Merge
d
P=7.88×10-3
P=3.17×10-5
P=9.62×10-5
P=8.08×10-3
P=1.56×10-2
P=2.93×10-4
e
PI4P
PI4,5P2
PI3,4,5P3
f
PIPn level
Cis
P=6.66×10-4
P=1.22×10-4
P=6.47×10-6
P=1.54×10-4
P=2.95×10-4
P=1.18×10-4
g
PIPKIα
sHSP
PI4P
PI4,5P2
PIPn-targets
p53
PI
PIPMK
PITPα/β
PTEN
PI3,4,5P3

Fig. 6

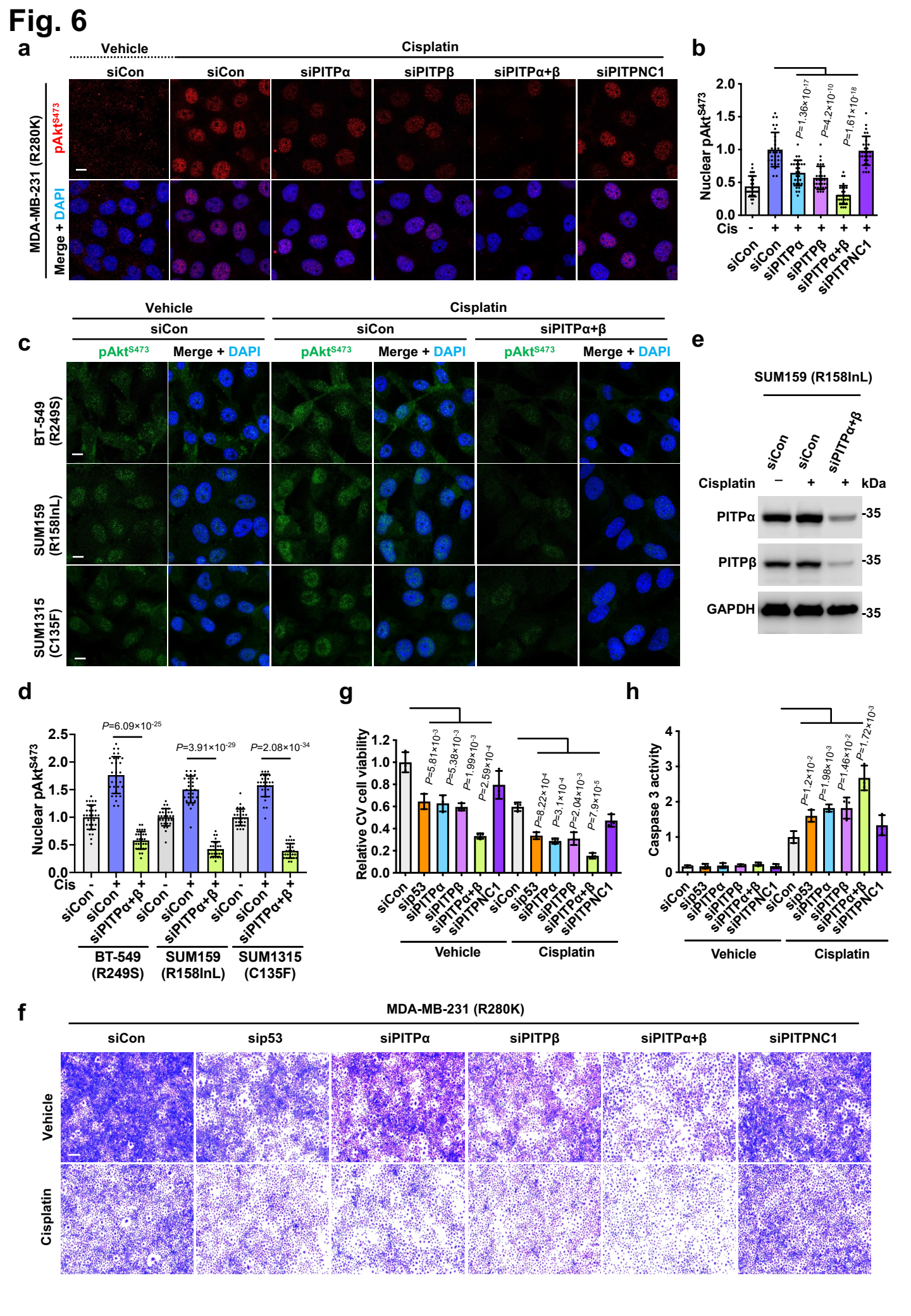
a
Vehicle
Cisplatin
siCon
siCon
siPITPα
siPITPβ
siPITPα+β
siPITPNC1
MDA-MB-231 (R280K)
pAkt^S473
Merge + DAPI
b
Nuclear pAkt^S473
P=1.36×10^-17
P=4.2×10^-10
P=1.61×10^-18
Cis
c
Vehicle
Cisplatin
siCon
siCon
siPITPα+β
pAkt^S473
Merge + DAPI
BT-549 (R249S)
SUM159 (R158InL)
SUM1315 (C135F)
e
SUM159 (R158InL)
siCon
siCon
siPITPα+β
Cisplatin
kDa
PITPα
PITPβ
GAPDH
-35
d
Nuclear pAkt^S473
P=6.09×10^-25
P=3.91×10^-29
P=2.08×10^-34
siPITPα+β
BT-549 (R249S)
SUM159 (R158InL)
SUM1315 (C135F)
g
Relative CV cell viability
P=5.81×10^-3
P=5.38×10^-3
P=1.99×10^-3
P=2.59×10^-4
P=8.22×10^-4
P=3.1×10^-4
P=2.04×10^-3
P=7.9×10^-5
siCon
sip53
siPITPα
siPITPβ
siPITPα+β
siPITPNC1
Vehicle
Cisplatin
h
Caspase 3 activity
P=1.2×10^-2
P=1.98×10^-3
P=1.46×10^-2
P=1.72×10^-3
f
MDA-MB-231 (R280K)
siCon
sip53
siPITPα
siPITPβ
siPITPα+β
siPITPNC1
Vehicle
Cisplatin

Extended Data Fig. 6

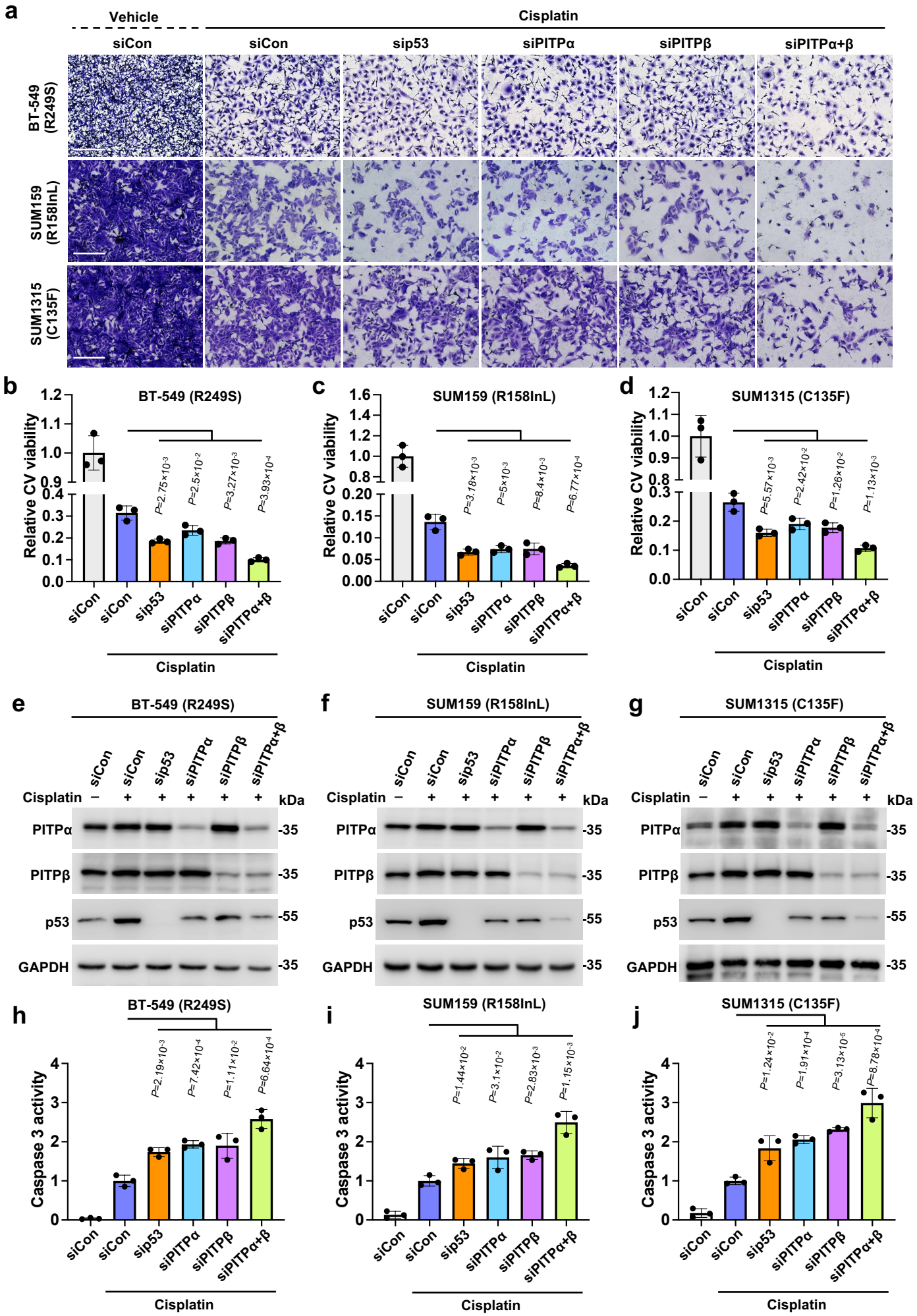

Fig. 7

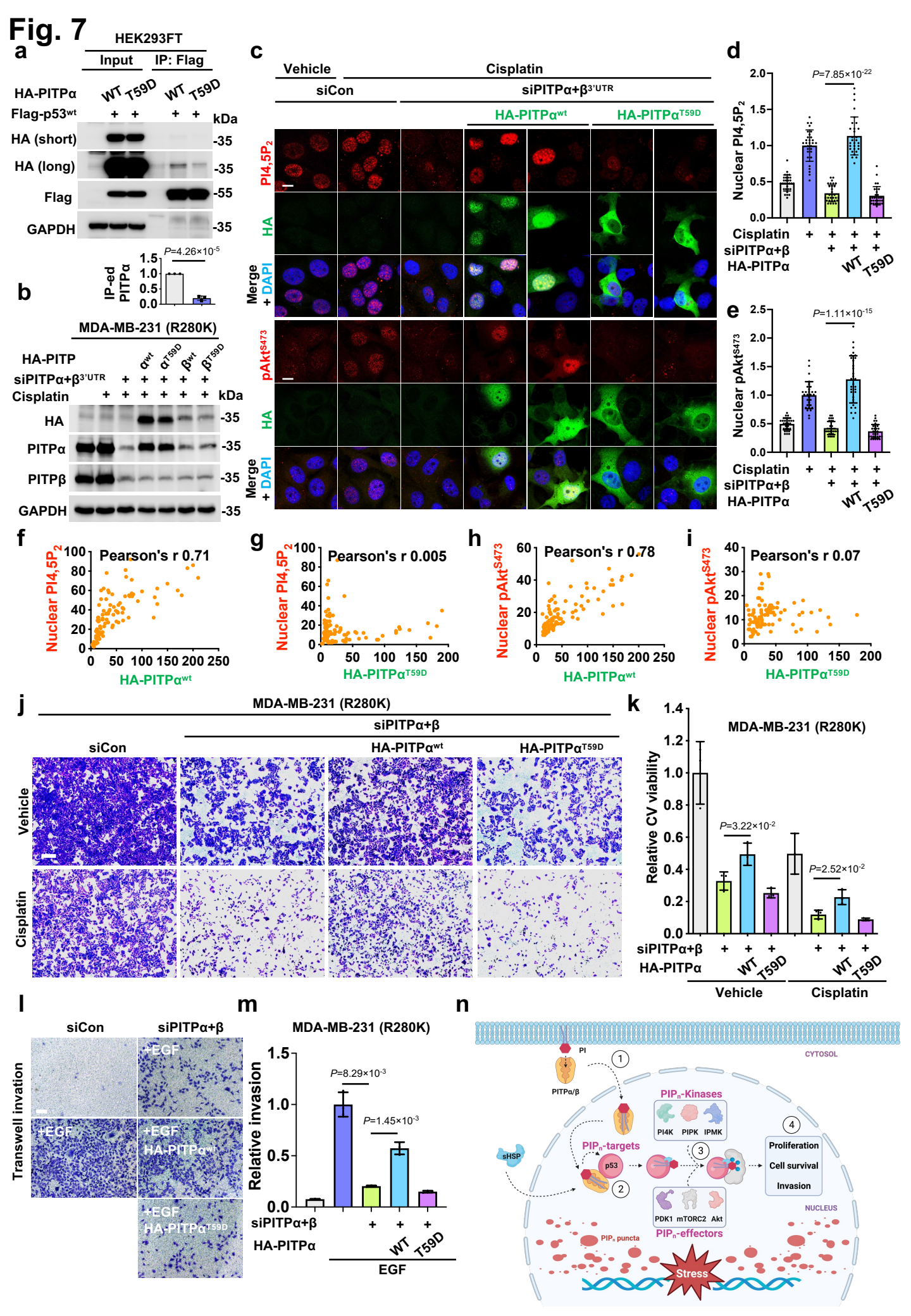
a
HEK293FT
Input
IP: Flag
HA-PITPα
WT
T59D
Flag-p53wt
kDa
HA (short)
HA (long)
Flag
GAPDH
-35
-55
b
IP-ed PITPα
P=4.26×10-5
MDA-MB-231 (R280K)
HA-PITP
αwt
αT59D
βwt
βT59D
siPITPα+β3'UTR
Cisplatin
HA
PITPα
PITPβ
GAPDH
c
Vehicle
Cisplatin
siCon
siPITPα+β3'UTR
HA-PITPαwt
HA-PITPαT59D
PI4,5P2
HA
Merge + DAPI
pAktS473
d
Nuclear PI4,5P2
P=7.85×10-22
Cisplatin
siPITPα+β
HA-PITPα
WT
T59D
e
Nuclear pAktS473
P=1.11×10-15
f
Pearson's r 0.71
Nuclear PI4,5P2
HA-PITPαwt
g
Pearson's r 0.005
HA-PITPαT59D
h
Pearson's r 0.78
Nuclear pAktS473
HA-PITPαwt
i
Pearson's r 0.07
HA-PITPαT59D
j
MDA-MB-231 (R280K)
siPITPα+β
siCon
HA-PITPαwt
HA-PITPαT59D
Vehicle
Cisplatin
k
MDA-MB-231 (R280K)
Relative CV viability
P=3.22×10-2
P=2.52×10-2
siPITPα+β
HA-PITPα
WT
T59D
Vehicle
Cisplatin
l
siCon
siPITPα+β
Transwell invation
+EGF
+EGF HA-PITPαwt
+EGF HA-PITPαT59D
m
MDA-MB-231 (R280K)
Relative invasion
P=8.29×10-3
P=1.45×10-3
siPITPα+β
HA-PITPα
WT
T59D
EGF
n
CYTOSOL
PI
PITPα/β
PIPn-Kinases
PI4K
PIPK
IPMK
sHSP
PIPn-targets
p53
Proliferation
Cell survival
Invasion
PDK1
mTORC2
Akt
PIPn-effectors
NUCLEUS
PIPn puncta
Stress
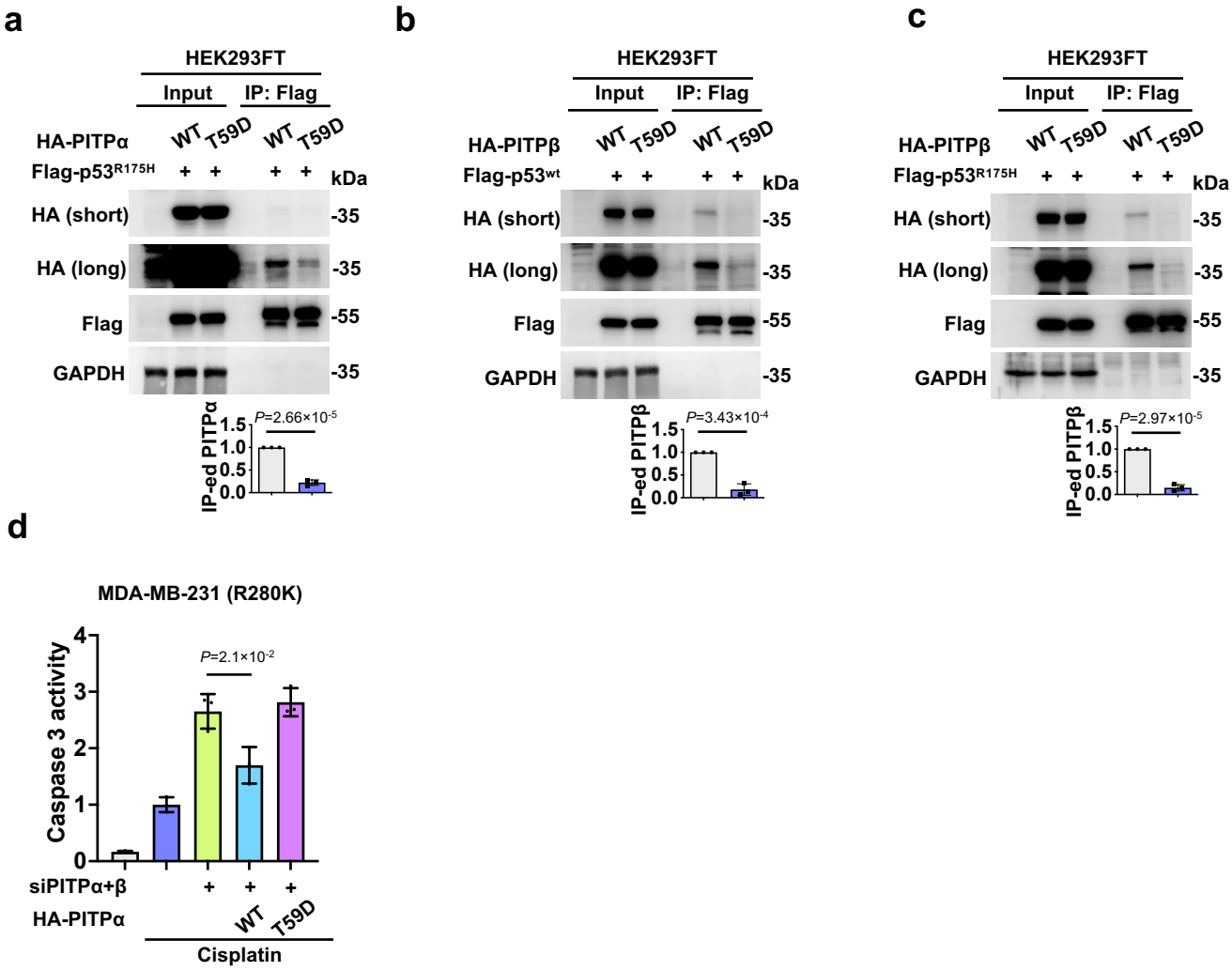
Extended Data Fig. 7